Microstructures and Late-Stage Magmatic Processes in Layered Mafic Intrusions: Symplectites from the Sept Iles Intrusion, Quebec, Canada

Halley A. Keevil[1],[2] Olivier Namur[1,3], and Marian B. Holness[1]

1. Department of Earth Sciences, University of Cambridge, Downing Street, Cambridge, United Kingdom, CB2 3EQ
2. Corresponding Author. Department of Geology and Geological Engineering, Colorado School of Mines, 1516 Illinois Street, Golden, CO, USA, 80401. E-mail: hkeevil@alumni.mines.edu. Phone: +1-778-773-8661.
3. Department of Earth and Environmental Sciences, KU Leuven, Heverlee, Belgium 3001

ABSTRACT

Replacive symplectites (vermicular intergrowths of two or more minerals) are an important feature of layered igneous intrusions, recording evidence of late-stage reactions between interstitial liquid and crystals. They are common throughout the Layered Series of the 564 Ma Sept Iles layered intrusion in Quebec, Canada, and fall into three types: oxy-symplectites, 'Type I' symplectites, and 'Type II' symplectites. Oxy-symplectites are comprised of magnetite and orthopyroxene, nucleate on olivine primocrysts, and form via the reaction Olivine + O_2 → Orthopyroxene + Magnetite; Type I symplectites (of which there are 3 distinct categories) are comprised of anorthitic plagioclase with pyroxene, amphibole, or olivine vermicules, grow from primocryst oxide grains, and replace primary plagioclase; and Type II symplectites (of which there are 2 distinct categories) are comprised of anorthitic plagioclase with orthopyroxene ± amphibole vermicules, grow from primocryst olivine

grains, and replace primocryst plagioclase. Rare symplectites composed of biotite and plagioclase are also present.

Symplectite growth occurred at 700-1030°C with pressure constraints of 1-2 kbar. We propose that Type I symplectites, and some Type II symplectites, formed from interaction of primocrysts with residual Fe-rich liquid as a consequence of differential loss of an immiscible Si-rich liquid conjugate from the crystal mush. However, redistribution and concentration of hydrous fluids in incompletely solidified rock, or an increase in water activity of the interstitial melt, may be more plausible processes responsible for the formation of replacive symplectites comprising abundant hydrous mineral assemblages.

KEY WORDS: Crystal Mush; Layered Mafic Intrusions; Microstructures; Sept Iles; Symplectites

INTRODUCTION

Detailed studies of volcanic rocks worldwide show that crystals found in lavas are often in disequilibrium with their carrier melts (Passmore *et al.,* 2012). This, together with theoretical modelling (Huber *et al.,* 2010), was used to argue that crustal magma reservoirs are long-lived features dominated by crystal mushes rather than by large, melt-rich, magma chambers (Cashman *et al.,* 2017). The presence of several crystal populations in lavas can thus be explained by the disaggregation of crystal mushes by injection of primitive melt, leading to the possibility of complex chemical interactions between existing mush and the incoming magma (Huber *et al.,* 2010; Kent *et al.,* 2010; Passmore et al., 2012; Neave *et al.,* 2014). Additionally, although some mafic layered intrusions such as Skaergaard in East Greenland most likely crystallized from a large magma body (McBirney, 1996), other mafic intrusions record evidence for multiple magma injections (e.g. Ashwal *et al.,* 2005; Namur *et al.,* 2010; Yuan *et al.,* 2017). These injections are commonly associated with geochemical and textural evidence for interaction between existing crystals and the incoming magma, such as mineral dissolution ± recrystallization due to percolation of interstitial melt (Humphreys, 2011; Namur *et al.,* 2013; Leuthold *et al.,* 2014).

In mafic intrusions crystallized from parent ferrobasalt, silicate liquid immiscibility is known to develop during differentiation (Holness *et al.,* 2011; Charlier *et al.,* 2011; Namur *et al.,* 2012*a*; Fischer *et al.,* 2016). Although the effect of basaltic or rhyolitic melt percolation on crystal mush melting and disaggregation is fairly well known (Lissenberg *et al.,* 2013; Bachmann & Huber, 2016; Yang *et al.,* 2019), comparatively little information is known about the percolation of extremely Fe-rich melts formed by silicate liquid immiscibility (Holness *et al.,* 2011; Namur *et al.,* 2012*a*). This type of melt can, however, be in very strong

chemical disequilibrium with the crystal matrix with an associated capacity for crystal dissolution, therefore promoting mush disaggregation and perhaps crystal entrainment.

Here we report the results of a detailed microstructural and geochemical study of symplectites in the Sept Iles intrusion, which we argue shed light on the extent and nature of reactive dissolution and reprecipitation within the crystal mush in slowly-cooled intrusions, with implications for element mobility and magma differentiation.

PREVIOUS CONSIDERATION OF SYMPLECTITE FORMATION

Symplectites are "reaction microstructures characterized by fine-grained vermicular intergrowths of two or more minerals (Spruzeniece *et al.,* 2017). Most research on symplectites has been conducted on metamorphic rocks, as symplectites are commonly formed in the sub-solidus at the interface of two reactive phases (e.g. Pitra & de Waal, 2001; Ikeda *et al.,* 2007; Scott *et al.,* 2013; Spruzeniece *et al.,* 2017). Due to their abundance in metamorphic rocks, symplectites observed in unmetamorphosed igneous rocks are still usually described as sub-solidus reaction products (e.g. Turner & Stüwe, 1992; Scott *et al.,* 2013; Spruzeniece *et al.,* 2017; Xie *et al.,* 2017). However, symplectites have been documented in unmetamorphosed oceanic gabbros (Koepke et al., 2005*a*; *b*; 2014; Lissenberg & MacLeod, 2016); the Skaergaard intrusion, East Greenland (Holness *et al.,* 2011); the Bushveld Complex, South Africa (Roelofse & Ashwal, 2008; Tanner *et al.,* 2014); the Duluth Complex, Minnesota (Gál *et al.,* 2011); the Panzhihua intrusion, China (Wang *et al.,* 2018); and the Sept Iles intrusion of Quebec, Canada (Namur *et al.,* 2012*a*).

Detailed chemical and microstructural investigation of these previously neglected replacive microstructures led Holness *et al.* (2011) to argue that symplectites can provide a record of

the extent of differential migration of immiscible interstitial liquids in gabbros. This is an important result because, despite much effort directed at understanding the liquid line of descent of basaltic magma during differentiation, little attention has been focussed on the evolution of the interstitial liquid within the crystal mush, particularly during the last stages of solidification when porosity and permeability are low (e.g. Boudreau *et al.,* 1986; Boudreau & McCallum, 1989; Meurer *et al.,* 1997; Meurer & Meurer, 2006; Humphrey, 2009; 2011; Namur & Charlier, 2012; Namur *et al.,* 2014; Namur & Humphreys, 2018). In the following, we describe the common types of replacive symplectites found in igneous rocks.

Oxy-symplectites

Oxy-symplectites comprise vermicules of an oxide phase (magnetite ± ilmenite or other spinels) enclosed by a mafic phase, most commonly orthopyroxene, although amphibole and occasionally clinopyroxene may also be present (e.g. Ikeda *et al.,* 2007; Holness *et al.,* 2011). They have been documented in many igneous environments, but there is no general consensus on their formation. They have been ascribed variously to nucleation and growth during sub-solidus cooling (Efimov & Malitch, 2012), exsolution (Moseley, 1984), metasomatic replacement reactions (Putnis & Austrheim, 2010), and late-stage magmatic (super-solidus) reactions with residual liquid during the latest stages of crystallization (Holness *et al.,* 2011).

Anhydrous Symplectites

Anhydrous symplectites generated in the super-solidus may simply result from the crystallization of pockets of late-stage liquids saturated in multiple phases (i.e. not involving reaction with pre-existing solid phases; Morse & Nolan, 1984; Gál *et al.,* 2011; Barnes *et al.,* 2017). Alternatively, they could form by reaction of infiltrating liquids with pre-existing phases (Irvine, 1980; Roelofse *et al.,* 2009), possibly by the reaction of a dense Fe-rich

immiscible interstitial liquid with the surrounding primocrysts caused by the preferential loss of the Si-rich conjugate (Holness *et al.*, 2011; Humphreys, 2011; Namur *et al.*, 2012*a*).

Hydrous Symplectites

Biotite- or amphibole-bearing symplectites are commonly observed in mafic igneous rocks. Although they have been attributed to post-magmatic (i.e. sub-solidus) hydration reactions (Turner & Stüwe, 1992; Xie *et al.*, 2017), a super-solidus origin has also been proposed via either reactions between primocrysts and a late-stage volatile phase in the final stages of crystallization of silicate melt (i.e. reactive porous flow; Lissenberg & MacLeod, 2016; Barnes *et al.*, 2017), or crystallization of partial melts triggered by hydrous fluid infiltration into partially solidified rocks (Koepke *et al.*, 2005*a*; *b*; 2014; Wolff *et al.*, 2013).

GEOLOGICAL BACKGROUND

The Sept Iles intrusion is a ferrobasaltic layered mafic intrusion located 500 km northeast of Quebec City in Quebec, Canada (Fig. 1; Higgins, 2005). It has a diameter of 80 km, a minimum thickness of 5.5 km, and an estimated magma volume of 20,000 km^3 (Loncarevic *et al.*, 1990), making it the third largest layered intrusion in the world after the Bushveld and Dufek intrusions (Namur *et al.*, 2010; Namur *et al.*, 2015). It formed contemporaneously with the opening of both the St. Lawrence rift system and the Iapetus Ocean (Kumarapeli & Saull, 1966) and was intruded into high-grade gneisses of the Archean to Mesoproterozoic Grenville Province at 564 ± 5 Ma (Higgins & van Breemen, 1998). The Sept Iles intrusion crops out on the north shore of the present-day St. Lawrence River and is entirely undeformed and unmetamorphosed (Namur *et al.*, 2010). Sr-Nd isotopic compositions are consistent with a

mantle source for the magma (Higgins & Doig, 1981) with minor crustal contamination (Namur *et al.*, 2011*a*).

About 90% of the volume of the intrusion is hidden beneath the St. Lawrence River, but two sets of deep drill cores (drilled by Inco Inc. and curated by the Ministère des Ressources Naturelles et de la Faune du Québec; Namur *et al.*, 2010) and the 30° dip of the margins of the intrusion towards the centre enable most of the stratigraphy of the intrusion to be accessed (Fig. 1; Namur *et al.*, 2010). Three different magmatic series have been described: the Layered Series, the Upper Border Series, and the Upper Series (Higgins, 2005; Namur *et al.*, 2010). The Upper Series forms cupolas at the top of the intrusion and comprises mainly A-type granite, likely to have resulted from fractional crystallization of the Fe-rich parent magma (Higgins, 2005; Namur *et al.*, 2011*a*). The Upper Border Series sits below the Upper Series and comprises anorthosites with minor leucogabbros and leuco-troctolites, likely resulting from flotation of plagioclase to the intrusion's roof (Namur *et al.*, 2011*b*). The Layered Series, which is the focus of this study, is at least 4.7 km thick and consists of troctolites, Fe-Ti oxide-bearing troctolites, and layered gabbros (Namur *et al.*, 2010). The layering in the Sept Iles is typical of layered mafic intrusions. The Layered Series, however, locally contains abundant centimeter- to meter-scale anorthosite blocks that deform the underlying layering (Namur *et al.*, 2010).

The Layered Series is subdivided into three megacyclic units: MCU I, MCU II, and MCU III, which show the following succession of cumulus assemblages (Namur *et al.*, 2010; 2012*a*; Fig. 1): troctolite consisting of plagioclase and olivine (po-C; p = plagioclase; o = olivine; classification scheme from Irvine, 1982); Fe-Ti oxide-bearing troctolite consisting of plagioclase, olivine, and Fe-Ti oxides (pomi-C; m = magnetite; i = ilmenite); and gabbro consisting of plagioclase, Fe-Ti oxides, clinopyroxene, ± olivine, ± apatite (pmic-C, pomic-C, and pomica-C; c = clinopyroxene; a = apatite). Both MCU I and MCU II are topped by a layer

of apatite-rich gabbro (Namur et al., 2010). The 200 m thick apatite-bearing layer near the top of MCU II contains nelsonite layers and is known as the "Critical Zone" due to the presence of potentially economic phosphorous and titanium (Cimon, 1998; Namur *et al.*, 2010). In the Layered Series stratigraphy, the '0 metre' reference level is defined as the lowermost apatite-bearing level of the Critical Zone (Namur *et al.*, 2010).

MCU I is 1785 m thick and dominated by troctolites and Fe-Ti bearing troctolites (po-C and pomi-C). The lowest part of the unit (with its base at -4200 m) crystallized cotectic proportions of olivine and plagioclase (Toplis and Carroll, 1995; Thy *et al.*, 2006). Magnetite and ilmenite become cumulus phases between -3600 m and -3400 m, followed by clinopyroxene at -3500 m. In the upper 200 m of MCU I, apatite becomes a cumulus phase. This apatite-bearing zone is 150 m thick and is composed of a unimodal, homogeneous apatite-bearing gabbro with plagioclase, olivine, clinopyroxene, magnetite, ilmenite, and apatite as cumulus phases (Namur *et al.*, 2012*a*). At the base of MCU I there is a marginal reversal about 60 m thick in the plagioclase, olivine, and Ca-rich pyroxene compositions: An_{63-68}, Fo_{68-72}, and Mg# 76-69, respectively. Above this reversal all phases become progressively more evolved upwards in the stratigraphy, reaching An_{47}, Fo_{55}, and Mg# 68 at the top of MCU I.

MCU II has a thickness of 2553 m and began crystallizing from a mixture of residual MCU I magma with a new injection of primitive parent magma (Namur *et al.*, 2010). Unlike MCU I, the evolution trend is characterized by numerous reversals to more primitive mineral compositions, each inferred to mark an injection of new magma. After the last magma injection, the compositions of plagioclase, olivine, and clinopyroxene evolve to An_{34}, Fo_{21}, and Mg# 55, respectively, at the top of MCU II. These mineral compositions are the most evolved in the intrusion, and Namur *et al.* (2010) suggest this is due to a longer differentiation interval than that for MCU I. The appearance of cumulus apatite at the base of the Critical

Zone occurs in the last 252 m of MCU II (Namur *et al.*, 2010). The Critical Zone contains the same minerals as the uppermost cumulates in MCU I, but differs from MCU II cumulates in that they are strongly bimodal, with leucocratic gabbros interlayered with melanocratic gabbros dominated by Fe-Ti oxides. This zone also contains abundant pigeonite, which is absent in the apatite-bearing horizon of MCU I (Namur *et al.*, 2012*a*). As described below, these rocks have been interpreted as having crystallized from alternating layers of Fe-rich (ca. 40% SiO_2, 20% FeO_t) and Si-rich (ca. 60% SiO_2, 40% FeO_t) immiscible melts (Charlier *et al.*, 2011).

The base of MCU III is thought to mark the arrival of a major batch of replenishing magma in the Sept Iles magma chamber (Namur *et al.*, 2010). The upper contact of MCU III is not exposed, but occurs at a stratigraphic height of at least 396 m according to Namur *et al.* (2010). The lithologies of MCU III are more similar to MCU I than MCU II. Ca-rich clinopyroxene is not a cumulus phase and the cumulates are dominated by troctolites and Fe-Ti oxide-rich troctolites. From the base to the top of the observed stratigraphy, plagioclase, olivine, and clinopyroxene show a progressive change to An_{70}, Fo_{70}, and Mg# 73, respectively (Namur *et al.*, 2010). Namur *et al.* (2010) suggested that the hybrid magma was formed by a primitive magma reacting with a lower proportion of residual magma from MCU II, whereas the replenishing magma at the base of MCU II reacted with a higher proportion of residual magma from MCU I.

Namur *et al.* (2012*a*) presented a forward model of the Sept Iles liquid line of descent for major elements in equilibrium with MCU I and MCU II cumulates. These authors argued that both these units formed from liquids which evolved towards enrichment in SiO_2 and depletion in FeO_t after saturation of Fe-Ti oxides. They also suggested that the melt in MCU I never unmixed, whereas the melt of MCU II entered a two-liquid field. The main reason why MCU I did not enter a two-liquid field is because the major event of magma replenishment that

formed MCU II took place before the MCU I melt was sufficiently evolved to encounter the two-liquid field. In addition, the magma mixing events in MCU II changed the evolution trend, particularly as the concentration of some elements was sufficient to enlarge the two-liquid field to enable the MCU II liquid to begin to unmix just before apatite saturation (Charlier *et al.*, 2011; Namur *et al.*, 2012*a*). After extensive fractionation associated with the formation of apatite-bearing cumulates (pomica-C), the bulk MCU II magma left the immiscible field, leading to the formation of a homogeneous melt only slightly more evolved than the immiscible liquids (Charlier *et al.*, 2011; Charlier *et al.*, 2013). This homogeneous melt was extracted from the Layered Series to form the granitic Upper Series (Namur et al., 2011*a*). This suggests that some parts of the crystal mush were still highly porous and permeable after the magma left the two-liquid field.

The record of immiscibility and unmixing in fully solidified mafic magma chambers is usually difficult to identify unambiguously and is commonly only represented by melt droplets trapped in (Jakobsen *et al.*, 2005), or between (Holness *et al.*, 2011; Humphreys, 2011), crystals. In Sept Iles, however, immiscible melts in MCU II underwent large-scale unmixing and segregation, resulting in the formation of metre-scale bimodal layering of alternating melanogabbro and leucogabbro in the upper part of MCU II, as well as forming compositionally contrasting apatite-hosted melt inclusions (Charlier *et al.*, 2011). This evidence for immiscibility of the bulk magma suggests that the interstitial liquid in the MCU II crystal mush likely encountered the binodal as well.

Although the main magma body in MCU I did not unmix, mixing of interstitial melts at different stages of evolution in the crystal mush, as well as their extensive fractionation, may have also led the interstitial liquid in MCU I to locally encounter the binodal and form two immiscible conjugates.

SAMPLES AND METHODS

285 samples from the Sept Iles Layered Series were examined for this study. Most of the samples from MCU I and MCU II are derived from two drill cores (120 samples from core DC-9 and 93 samples from core DC-8), from which samples were taken every 10 or 40 m. An additional set of 42 samples was collected from the apatite-bearing gabbro horizon of MCU II (stratigraphic height of 0 to 193 m), sampled by drill core S-9 provided by Soquem Inc. (Namur *et al.*, 2012*a*). The remaining samples were collected from surface outcrop in 2007, using precise GPS and altimeter data: these are currently curated by the Department of Geology at the University of Liège, Belgium.

Petrography

Polished thin sections were examined using a Nikon Eclipse E600 POL petrographic microscope at the Department of Earth Sciences at the University of Cambridge. Photomicrographs were obtained with a Nikon Coolpix 5000, using a Coolpix MDC Lens. Back-scatter electron (BSE) images were obtained using a JEOL 820 Scanning Electron Microscope (SEM) in the Department of Earth Sciences at the University of Cambridge. SEM operating conditions were 20 kV accelerating voltage with a 1 nA beam current at a working distance of 15 mm.

Colour cathodoluminescence images were obtained using an in-house cold-cathode instrument. An accelerating potential of ~26 kV generated a gun current of 450-600 mA with an air chamber pressure of 0.01-0.05 Torr. The gun is equipped with a focussing coil to gain high magnification images. The chamber sits on a Nikon Optiphot optical microscope and is connected to an Optronics Magnafire peltier-cooled digital camera. Prior to the capturing of photographs, the white balance of the camera was adjusted using the program “MagnaFire” to

give maximum definition. As a result, the images are not an accurate record of colour wavelength, but qualitatively demonstrate the different wavelengths of luminescence.

Electron Microprobe Analyses

Mineral compositions were determined using a Cameca SX-100 electron microprobe at the Department of Earth Sciences at the University of Cambridge. Operating conditions for feldspars were 15 kV accelerating voltage, 10 nA beam current, and a 1 μm beam size. Operating conditions for amphibole, biotite, pyroxenes, olivine, and oxides were 15 kV accelerating voltage, 20 nA beam current, and a 1 μm beam size.

Standards used were diopside for Si and Ca, rutile for Ti, corundum for Al, fayalite for Fe, Mn for Mn, olivine (San Carlos) for Mg, jadeite for Na, K-feldspar for K, celestite for Sr, fluorite for F, halite for Cl, Cr for Cr, and NiO for Ni. Counting times were 20 seconds on peak and 10 seconds for background on each side of the peak for major elements, and 60 seconds on peak and 30 seconds for background for minor elements. Raw data have been corrected with the CATZAF software, included in the Cameca software.

Mass Balance

Mass balance calculations to reconstruct average symplectite compositions were performed using compositions obtained with the electron microprobe, together with modal analyses obtained from BSE images. The volume percent of each mineral phase in the symplectite (± the surrounding rim) was calculated by averaging modes obtained by analysis of over 50 SEM images using the program ImageJ. Two-dimensional proportions were assumed to be representative of those in three dimensions. To convert volume percent into weight percent, we used densities of each mineral calculated from chemical compositions. Bulk symplectite

compositions were determined by combining out volumetric measurements with the elemental oxide compositions of each mineral: results were compared to bulk rock compositional data.

Thermometry

We used the hornblende-plagioclase thermometer "Hb-Pl" from Holland & Blundy (1994) to determine the symplectite crystallization temperatures. Although designed for metamorphic rocks, the program works well for a broad range of compositions, and performs well (±40°C) in the range of 400-1000°C and 1-5 kbar (Holland & Blundy, 1994). The QUILF geothermometer (Andersen *et al.,* 1993) was used to determine reaction temperatures for clinopyroxene-orthopyroxene symplectites, assuming pressures of 1-2 kbar (Namur *et al.,* 2010). Biotite laths rooted to oxide grains (some of them forming symplectic structures with plagioclase) were also used to determine temperatures: we used the method of Henry *et al.* (2005), which has been shown to be accurate for mafic rocks (Namur *et al.,* 2009). The possibility of sub-solidus re-equilibration of co-existing phases means that calculated temperatures may represent the closing temperature of the system, and are therefore minimum estimates.

SYMPLECTITE CLASSIFICATION AND STRATIGRAPHIC DISTRIBUTION IN THE SEPT ILES LAYERED SERIES

In the Sept Iles Layered Series, the replacive symplectites vary in terms of the root primocryst, the presence and composition of a rim around the root primocryst, and the minerals comprising the symplectite. The symplectites were subdivided into three main types: oxy-symplectites that replace olivine (Table 1; Fig. 2); Type I symplectites that are rooted to oxide grains and replace primocrysts of plagioclase (Table 1; Fig. 3); and Type II symplectites that also replace primocryst plagioclase but are rooted to olivine grains (Table 1; Fig. 4; c.f.

Holness *et al.*, 2011). Most of these symplectites are similar to those described in the Skaergaard intrusion (Holness *et al.*, 2011). There are also more uncommon symplectites observed in the Sept Iles intrusion, composed only of biotite and plagioclase (Table 1; Fig. 4c). No equivalent symplectites were observed in Skaergaard. The Type I and Type II symplectites have been further subdivided to create five distinct categories. In all reactive symplectites, there is no textural evidence to suggest that phases other than plagioclase were replaced during the symplectite-forming process. The stratigraphic distribution of all symplectites is given in Figure 5.

Oxy-symplectites

Oxy-symplectites are composed of orthopyroxene enclosing individual magnetite (± ilmenite) vermicules, and replace primocryst olivine where adjacent to primocrysts of Fe-Ti oxide grains (Fig. 2). Oxy-symplectites are most common at the base of MCU I (po-C), becoming less abundant immediately after saturation in Fe-Ti oxides (pomi-C; Fig. 5). However, they are still present in small numbers throughout the upper part of MCU I and MCU II, where oxides are liquidus phases. They are slightly more common in MCU III, especially in the upper part, which is free of oxide primocrysts (po-C).

Type I Symplectites

Type I-a Symplectites

Type I-a symplectites are rooted to Fe-Ti oxide grains and are predominantly composed of orthopyroxene (± rare clinopyroxene) vermicules in an anorthitic matrix (Fig. 3a). They consume primocryst plagioclase. Rims may be absent on the oxide root but, more commonly, there is an orthopyroxene rim in optical continuity with orthopyroxene forming symplectite

vermicules. Biotite rims are commonly present at the margins of symplectite-bearing oxide grains (Fig. 3a), although there is no evidence that the mafic vermicules grow directly from the biotite rims. Similar symplectites were described in Skaergaard although they are not abundant (Holness *et al.*, 2011).

In Sept Iles, Type I-a symplectites are rare at the base of MCU I, but become abundant after saturation of Fe-Ti oxides (at a depth of ~-3680 m). They are abundant throughout MCU II but disappear near the base of the S-9 drill core (MCU II; pomica-C). They re-appear at the top of MCU II with a less organized structure, in which the mafic vermicules are variably sized and oriented, and are present throughout MCU III (Fig. 5).

Type I-b Symplectites

Type I-b symplectites differ from Type I-a in that they contain amphibole (magnesio-hornblende), both as rims surrounding the oxides and as vermicules within anorthitic plagioclase in the symplectite itself (Fig. 3b). In some symplectites of this group, the amphibole grades out along the growth direction into orthopyroxene ± clinopyroxene. Unlike other Sept Iles symplectites, the amphibole vermicules in Type I-b symplectites commonly do not extend to the edge of their anorthitic plagioclase host (Fig. 3b). The grain size in Type I-b symplectite vermicules is generally coarse throughout.

Type I-b symplectites are rare: they were found in three samples: ON-07-152 (pmic-C at -239 m), ON-07-155 (pmic-C at -114 m), and ON-07-156 (pmic-C at -80 m) at the top of MCU II, below the appearance of cumulus apatite (Fig. 5). This type of symplectite appears to be absent in Skaergaard.

Type I-c Symplectites

Type I-c symplectites are composed of olivine (which is locally replaced by clinopyroxene at the outer margins) and anorthitic plagioclase, and grow from olivine rims surrounding Fe-Ti oxide grains (Fig. 3c). They are found only in the region of stratigraphy covering the upper part of pomica-C cumulates at the top of MCU II, near the top of the S-9 drill core, and into the base of MCU III (Fig. 5). These symplectites are very similar to the common Type I symplectites described in Skaergaard (Holness *et al.,* 2011).

Type II Symplectites

Type II-a Symplectites

Type II-a symplectites are rooted to olivine grains with variably sized orthopyroxene rims, ± laths of a hydrous phase (usually annitic phlogopite, particularly in MCU I) (Fig. 4a). The symplectite vermicules are composed predominantly of orthopyroxene, which may be replaced along the growth direction by clinopyroxene. Like most other symplectites in Sept Iles, the symplectite vermicules decrease in size along growth direction and terminate together with the anorthitic plagioclase host. Type II-a symplectites are similar to the Type 2 symplectites described in Skaergaard (Holness *et al.,* 2011).

Type II-a symplectites have a similar stratigraphic distribution to that of the oxy-symplectites (Fig. 5). In the lowest section of MCU I, they are common and are associated with annitic phlogopite as well as orthopyroxene rims. Above -3619 m (pomi-C), they are extremely rare but generally have (variably altered) orthopyroxene rims. They appear, albeit rarely, throughout MCU II and into MCU III, where there are numerous Type II-a symplectites observed that show a more irregular structure (Fig. 5).

Type II-b Symplectites

Type II-b symplectites are also rooted to olivine and replace primocryst plagioclase, but contain amphibole in the rim assemblage as well as orthopyroxene (Fig. 4b). The amphibole rim is commonly in optical continuity with the thick amphibole vermicules of the symplectite. The general trend (from the olivine primocryst to the outer edge of the symplectite) is: orthopyroxene rim → amphibole rim → amphibole-anorthite symplectite → orthopyroxene-anorthite symplectite → plagioclase primocryst (Fig. 4b). The amphibole vermicules, as in Type I-b symplectites, are wider and thicker than the orthopyroxene, clinopyroxene, or olivine vermicules in other symplectite types. They are also more irregular in shape and in spacing within the symplectic intergrowth. Type II-b symplectites contain a much larger amphibole fraction than any symplectite described in Skaergaard, including the Type 2 which may contain an amphibole rim (Holness *et al.*, 2011).

Type II-b symplectites are only found near the top of MCU III (Fig. 5).

Biotite-Plagioclase Symplectites

A rare type of symplectite in the Sept Iles intrusion is composed of biotite laths within anorthitic plagioclase, and replaces primocryst plagioclase. The biotite laths are usually rooted to Fe-Ti oxide grains, but they commonly appear with no oxide root (at least in the plane of the thin section) within plagioclase-rich areas, grading out into pyroxene-anorthite "Type I" symplectites along the growth direction (Fig. 4c). Biotite-plagioclase symplectites are common at around ~1000 m in MCU II (in pomi-C and pomic-C), and reappear sporadically throughout MCU III.

SYMPLECTITE COMPOSITIONS

Oxy-symplectites

A single oxy-symplectite was analysed for orthopyroxene and magnetite compositions, as well as the surrounding olivine primocrysts (Fo_{64}; Fo = molar Mg/(Mg + Fe). The symplectic orthopyroxene yields an Mg# of 70 [Mg# = molar Mg/(Mg + Fe)], whereas the orthopyroxene in the rest of the sample yields a similar average Mg# of 69 (Namur *et al.*, 2010). No significant compositional variations were observed in the oxy-symplectites. The oxide in the symplectite is, on average, 85% magnetite and 15% ülvospinel, whereas in the rest of the sample the oxides are generally ~80% magnetite (Supplementary Information 1). Note that bulk oxide compositions were obtained by X-ray fluorescence on mineral separates rather than by electron microprobe analyses (Namur *et al.*, 2010).

Type I Symplectites

Type I-a Symplectites

The plagioclase composition in Type I-a symplectites averages An_{80} [An = molar Ca/(Ca + Na)] throughout the Layered Series, with compositions up to An_{96}. There are no well-defined and consistent compositional spatial variations in anorthite content within each symplectite (Supplementary Information 2). Instead, the An-content varies in distinct “pulses” and can either monotonically increase or decrease, or oscillate along the growth direction. The composition can vary by up to 30 mol.% An within a symplectite (Fig. 6a).

Unlike the plagioclase, the orthopyroxene in Type I-a symplectites shows consistent compositional trends. That in the symplectite has an initial composition similar to that of the orthopyroxene rim (if present), before decreasing systematically in Mg# by an average of 1-3 mol.% (and maximum 5-6 mol.%) along the growth direction (Fig. 6a). If no rim is present,

the initial Mg# of the symplectite orthopyroxene is within 1 mol.% of the orthopyroxene typical of that part of the Layered Series (Namur *et al.,* 2010).

Type I-b Symplectites

Type I-b symplectites show similar patterns of An-content and Mg# to other types of symplectites. Symplectite plagioclase may be as anorthitic as An_{80} (with an average of An_{77}) whereas the most anorthitic plagioclase in the surrounding primocrysts is An_{64}. The largest observed difference between symplectic plagioclase and primocryst plagioclase is 27 mol.% (Fig. 6b). Plagioclase composition within the symplectite does not vary systematically along the growth direction, with irregular patches of variably anorthitic plagioclase.

The Mg# of the amphibole in the symplectite generally decreases along the growth direction, although there are symplectites that maintain a similar Mg# along growth direction (Supplementary Information 3). At the start of growth, the Mg# is always the same as the rim on which it is rooted (ranging between 66-75). The decrease in Mg# is never more than 5 mol.% (Fig. 6b; Supplementary Information 3).

Type I-c Symplectites

The plagioclase in Type I-c symplectites is highly anorthitic with no consistent spatial variations. Despite plagioclase primocrysts having average compositions of ~$An_{45,}$ the anorthite content in these symplectites can be as high as An_{88}. Like Type I-b symplectites, irregular patches of variably anorthitic plagioclase occur throughout the symplectite, with the adjacent primocryst up to 48 mol.% poorer in anorthite than the symplectic plagioclase (Fig. 6c).

The olivine in the symplectite initially grows with a composition almost identical to that of the rim (Supplementary Information 4). As growth proceeds, the olivine composition generally becomes less forsteritic, but not as significantly so as in other symplectite types (ranging from Fo_{41}-Fo_{37}). Rarely, there is no systematic trend in Fo-content, with only a spatially random variation ranging around 2 mol.%, whereas in other Type I-c symplectites the Fo-content decreases by up to 4 mol.% along the growth direction (Fig. 6c).

Where present, clinopyroxene vermicules always occur on the outer margin of the symplectite (i.e. they grow after the olivine vermicules). The Mg# of the clinopyroxene in the symplectites ranges from 64 to 69, either decreasing by up to 1 mol.% along the growth direction or remaining the same. Clinopyroxene is usually only present in the outermost margins of the symplectite and the vermicules are commonly too narrow for microprobe analyses (<1 μm), so no growth trends were analysed.

Type II Symplectites

Type II-a Symplectites

Type II-a symplectites share similar trends to Type I symplectites. The symplectite plagioclase ranges from An_{73} to An_{95}, with an average of An_{80}. The difference in An-content between the symplectite and adjacent primocryst can reach up to 35 mol.%. Like the other symplectite types, plagioclase composition does not vary spatially in a systematic manner (Fig. 7a). Orthopyroxene, the most common mafic mineral in Type II-a symplectites, follows compositional trends similar to Type I symplectites, with decreasing Mg# along the growth direction. The decrease is usually on the order of 3-5 mol.% but can be up to 8 mol.% (Fig. 7a). Although the composition at the start of growth is typically almost identical to that of the orthopyroxene rim on which it is rooted, rarely the symplectite orthopyroxene starts with a

slightly lower Mg# than the rim (usually within ~0.5mol.%). Symplectite orthopyroxene ranges from Mg# 60 to 73.

Clinopyroxene vermicules in Type II-a symplectites are commonly very fine-grained and are quite rare, so little compositional data was collected. However, like the Type I-c symplectites, the decrease in Mg# with growth is not prominent. In Type II-a symplectites, the Mg# varies from 76 to 83 (Supplementary Information 5).

Type II-b Symplectites

The anorthite content of plagioclase in Type II-b symplectites ranges between An_{80} and An_{92}, with a difference of up to 35 mol.% compared to the adjacent primocryst (An_{55-61}). The average composition of the symplectite plagioclase is An_{86}. Although there are no well-defined and consistent compositional trends, the An-content generally decreases along the growth direction (Fig. 7b).

The orthopyroxene rims that surround the olivine root primocryst have an Mg# of 70-72. The Mg# of the amphibole vermicules varies from 67 to 71. A decrease in Mg# can occur with growth, but the maximum size of this decrease is only ~3 mol.% (Fig. 7b). The Mg# in those pyroxene vermicules large enough to analyse does not vary by more than 1 mol.% within the symplectite (Supplementary Information 6).

Biotite-Plagioclase Symplectites

The plagioclase within the biotite-plagioclase symplectites ranges from An_{71} to An_{95}, with an average composition of An_{79}. The adjacent primocrysts have compositions in the range An_{40-65}: the difference in anorthite content between the symplectite plagioclase and adjacent primocryst can reach 48 mol.%. The biotite vermicules in these symplectites do not show

consistent compositional trends, with the Mg# varying by up to 5 mol.% with growth (Fig. 7c; Supplementary Information 7).

CATHODOLUMINESCENCE IMAGES OF SYMPLECTITES AND PRIMOCRYSTS

The composition of plagioclase crystals and its thin section scale variability can be qualitatively assessed using colour cathodoluminescence images. All types of replacive symplectite, with the exception of the uncommon Type I-c and biotite-plagioclase symplectites, were studied using colour cathodoluminescence. We examined one representative thin section from each of the three MCUs: sample 9-2087.5 from MCU I contains abundant Type II-a symplectites; sample 8-1838.5 from MCU II contains abundant Type I-a symplectites (Fig. 8a); and sample ON-07-102 from MCU III contains abundant Type I-b and II-b symplectites (Fig. 8b). Representative cathodoluminescence images from these samples can be seen in Supplementary Information 8.

Two types of luminescence were observed: green luminescence that corresponds to high An-content (as verified by microprobe analyses) and blue luminescence that corresponds to a much lower An-content. In MCU I and MCU II, anorthitic plagioclase in the reactive symplectites luminesces green. In the same rocks, the lower An cores of the primocrysts luminesce blue. However, the grain boundaries between plagioclase primocrysts commonly luminesce green (Fig. 8a), indicating that the marginal few microns of plagioclase crystals are highly anorthitic.

The luminescent behaviour of plagioclase in MCU III is more complicated. Symplectite plagioclase in all types of symplectite commonly luminesces green due to high An-content, whereas the plagioclase primocrysts luminesce green or blue. Blue luminescence is mostly

observed in the central parts of crystals, as irregular patches of low-An material (Fig. 8b). Green luminescence correlates with areas of clear, less turbid plagioclase, and is also found at crystal margins. The boundary between green and blue luminescence is irregular and fingered. All microprobe data for symplectite and primocryst compositions are presented in Supplementary Information 8.

COMPARISONS BETWEEN SYMPLECTITES AND PRIMOCRYSTS

Symplectite plagioclase in all Type I, Type II, and biotite-plagioclase symplectites is significantly more anorthitic than the adjacent primocrysts (Fig. 9a), but is similar in composition with respect to other elements. Symplectite plagioclase contains almost no TiO_2 and K_2O (i.e. below microprobe detection limits or just above), compared to ~0.05-0.3 wt.% TiO_2 (possibly due to inclusions of oxides) and up to 1 wt.% K_2O in the primocrysts. The FeO content is slightly lower in primocrysts (average of 0.26 wt.% compared to 0.42 wt.% in symplectites). No spatial trends in symplectite plagioclase compositions, or in their relationship with primocryst compositions, occur on any scale, either within a single symplectite or on the scale of the Layered Series.

For both clinopyroxene and orthopyroxene, the compositional variation within symplectites is larger than the variation observed in the primocryst or rim compositions. The distribution of Mg# for clinopyroxene is shown in Fig. 9b. Comparison between the composition of clinopyroxene in symplectites and in primocrysts is difficult because clinopyroxene-bearing symplectites are only observed in two stratigraphic intervals: in the lower part of MCU I where clinopyroxene is not a cumulus phase (po-C and pomi-C), and in the most evolved cumulates (pomica-C) of MCU II. As a consequence, very few primocrysts of clinopyroxene

were present to measure in symplectite-bearing samples. In Fig. 9b, we therefore compare the compositions of clinopyroxene in symplectites with clinopyroxene primocrysts from the whole stratigraphic sequence as measured by Namur *et al.* (2010). We made two important observations: (1) clinopyroxene in symplectites from MCU I is more primitive (higher Mg#) than any clinopyroxene primocryst, consistent with these symplectites occurring in a stratigraphic unit without clinopyroxene primocrysts; (2) clinopyroxene in symplectites from the pomica-C cumulates of MCU II is evolved (Mg# 60-70) and identical to the compositions of the primocrysts observed in this stratigraphic unit (Namur *et al.*, 2010; 2012*a*). Although there is no cumulus orthopyroxene in the Sept Iles intrusion, except perhaps at the top of MCU II, there are many orthopyroxene rims surrounding primocryst grains of olivine and Fe-Ti oxides. These rims have a narrow compositional range, with Mg# of 69 to 74, whereas that of the symplectite orthopyroxene ranges from the same value as the rim down to Mg# 59 (Fig. 9c).

Primocryst olivine forms two populations, with one clustered around Fo_{45} (mostly from pomica-C samples from MCU II; Charlier *et al.*, 2011; Namur *et al.*, 2012*a*), and the other around Fo_{65} (from MCU I, II, and III: data from this study and from Namur *et al.*, 2010). It is likely that intermediate compositions between two populations exist at the bottom of the pomica-C unit of MCU II but were not sampled by Namur *et al.* (2012*a*). This is because, in this part of the intrusion, mineral compositions change rapidly with increasing stratigraphic height. Symplectic olivine was only observed in Type I-c symplectites that occur in the pomica-C unit of MCU II where olivine primocrysts are highly evolved (Fo < 45). Symplectic olivine is initially the same composition as the rim from which it grows. There is a slightly wider spread in symplectite composition compared to the primocryst, as it generally decreases by a few mol.% with growth (Fig. 9d). Apart from Fo-content, no clear compositional differences are found between the primocrysts and the symplectites.

No cumulus amphibole is present in the Sept Iles Layered Series, although this is a major phase in the Sept Iles Upper Series (granite). The Mg# of amphibole rims are in the range 63-80, with most being 70-72, whereas the symplectites show a similar compositional range but with a slightly lower average Mg# for the symplectites compared to the rims (Supplementary Information 3; 6; 10). The compositional trends of all other major and minor elements in the rims and symplectites of the same samples are generally similar, varying only within 1 wt.%.

MASS BALANCE

In order to retrieve bulk compositions, mass balance calculations were performed on 37 symplectites in which plagioclase primocrysts were replaced by anorthitic plagioclase and various mafic phases (pyroxene, olivine, or amphibole). The calculated symplectite bulk compositions were compared to the composition of the replaced plagioclase primocryst to determine which elements were gained or lost during reaction. Critical to these mass balance calculations is an accurate knowledge of the position of the original primocryst grain boundary. Although there is uncertainty in the position of the original primocryst boundary, and in the volume fraction of each mineral in the symplectites, we observe coherent results for all types of symplectites, suggesting that our mass balance calculations offer a relatively accurate estimate of bulk symplectite compositions. Note that the general trend in net gains and losses is relatively similar when calculations are performed with partial replacement of the root primocryst in addition to plagioclase (Supplementary Figure 1).

For Type I-a, Type I-b, and Type I-c symplectites, the position of the original grain boundary was chosen as the inner margin of the orthopyroxene, amphibole, or olivine rim, respectively. These mafic rims were included in the mass balance analyses as part of the symplectite

because the mafic mineral in the innermost part of the symplectite has the same composition as the rim, and the rims grade into the symplectite vermicules in most samples. For similar reasons to those described for the Type I symplectites, the inner boundary for both Type II-a and II-b symplectites was placed at the outer limit of the olivine primocryst.

Growth of all Type I symplectites involves a net loss of SiO_2, Al_2O_3, and Na_2O, with a net gain of FeO and MgO and either a slight net gain or loss of CaO (Fig. 10a-c). TiO_2, MnO, and K_2O do not change significantly. This is similar to the results of Holness *et al.* (2011) for Type I symplectites in the Skaergaard intrusion. The same general trends are observed for Type II-a and Type II-b symplectites (Fig. 10d and e).

Due to the scarcity of biotite-plagioclase symplectites and the small size of the biotite vermicules, only one symplectite of this type was analysed. It shows a net loss of SiO_2, Al_2O_3, CaO, Na_2O, and K_2O compared to the primocryst plagioclase surrounding it, with a net gain of TiO_2, FeO, and MgO.

THERMOMETRY

The compositions of amphibole rims and adjacent plagioclase primocrysts yield a temperature range of 737-932°C with an average of 852°C (48 pairs of points; Table 2; Supplementary Information 10) as calculated using the thermodynamic model of Holland & Blundy (1994). This model is expected to be accurate for temperatures in the range 400-900°C if the amphibole composition has Na > 0.02 pfu (per formula unit), $Al^{VI} < 1.9$ pfu, and Si in the range 6.0-7.7 pfu, associated with plagioclase with An < 0.90. These criteria are all fulfilled for the pairs of amphibole rims and adjacent plagioclase primocrysts studied here. Sixty-two calculations were performed for coexisting amphibole symplectites and anorthitic plagioclase,

yielding a temperature range of 784-1007°C with an average of 899°C (Table 2). These results should be treated with caution, however, because some values are outside the recommended temperature range and some symplectites contain plagioclase more anorthitic than An_{90}.

Clinopyroxene-orthopyroxene solvus geothermometry was applied to 6 samples containing both orthopyroxene and clinopyroxene in the same symplectite. K_D values for MgO-FeO exchange suggest that both phases are in chemical equilibrium (Toplis & Carroll, 1995). Temperatures obtained using the QUILF algorithm (Anderson *et al.*, 1993) range of 751-892°C with an average temperature of 821°C (average error of 32°C), whereas temperatures obtained with the model of Putirka (2008) range from 777 to 910°C with an average temperature of 835°C (Table 2). QUILF results should be treated with caution because QUILF is expected to be accurate for systems containing pyroxene, olivine, and quartz, but quartz is absent in the Sept Iles cumulates. However, we note that the results from QUILF are similar to those obtained with the model of Putirka (2008) for which equilibrium criteria ($Kd_{Fe-Mg}^{Cpx-Opx}$:1.09 ± 0.14) are fulfilled by Sept Iles clinopyroxene-orthopyroxene pairs. Temperatures were calculated at a pressure of 1 kbar, which Namur *et al.* (2011) estimated as the pressure at the top of the magma chamber. However, changing the pressure by 1 kbar changes the calculated temperatures by less than 3°C for either method.

Thermometry using the compositions of biotite laths rooted to oxide grains and in symplectite intergrowths was performed using the model of Henri *et al.* (2005), which is accurate for samples containing ilmenite (Namur *et al.*, 2009). This model yields temperatures ranging from 665°C to 980, with an average of 926°C (521 measurements) (Table 2). The lowest temperatures (in the 700-900°C range) are all from biotite rooted to olivine, regardless of their

location in the stratigraphy. The highest temperatures (comprising the majority of the data) are from biotite laths rooted to Fe-Ti oxide grains.

DISCUSSION

The results of the present study demonstrate seven clearly distinguishable types of late-stage replacive symplectites in the Layered Series of the Sept Iles intrusion, each with a different stratigraphic distribution. In the Sept Iles Layered Series, oxy-symplectites are most abundant in the lower part of MCU I and occur in rocks with no oxide primocrysts, decreasing in abundance after saturation of the bulk magma in Fe-Ti oxides. A similar stratigraphic distribution was found in the Skaergaard intrusion by Holness *et al.* (2011), who interpreted their formation as the result of an increase in oxygen fugacity in the residual liquid during the last stages of solidification, triggering the following reaction: Olivine + O_2 → Orthopyroxene + Magnetite. This reaction would form the mineral assemblages observed in oxy-symplectites from the Sept Iles intrusion, with textural and compositional relationships indicating the symplectites here formed in the same fashion as those at Skaergaard.

All other symplectite types in the Sept Iles intrusion involve the loss of Si, Al, and Na, and the gain of Fe and Mg, and therefore must have grown in an open system. This is consistent with cathodoluminescence images from MCU I and MCU II that show green luminescent plagioclase along grain boundaries, whereas the centres of plagioclase primocrysts luminesce blue. Since only the marginal few microns of plagioclase grains luminesce green and contain high anorthite content, simple chemical zoning during late-stage crystallization of intercumulus melt is not an adequate explanation. Instead, we suggest that the process that formed the high-An plagioclase in the symplectites also affected the rims of the plagioclase primocrysts. The blue patches probably represent relics of primocrysts crystallized from the

main magma body, whereas green areas are of anorthitic plagioclase that has grown via a replacement process similar to that which formed the symplectites. It is therefore likely that the distinct pattern of green luminescence demonstrates fluid or melt transport along grain boundaries in an open system.

The reactions that formed the reactive symplectites of the Sept Iles most likely occurred in the super-solidus, with the lower temperatures associated with biotite (665-980°C) corresponding to sub-solidus re-equilibration. As the majority of relatively high temperature estimates for biotite thermometry were obtained from biotite laths rooted on Fe-Ti oxide grains, however, we cannot exclude the possibility that these are a consequence of Ti diffusion from the oxide into the biotite.

The temperatures obtained by most of the thermometry calculations are at the boundary between super- and sub-solidus conditions (Thy *et al.*, 2009; Charlier & Grove, 2012; Charlier *et al.*, 2013). We do, however, note that at a pressure of 1-3 kbar, temperatures above 850°C would be super-liquidus for melts with water contents of 4-5 wt.% H_2O (Bogaerts *et al.*, 2006), expected in the most evolved, amphibole-crystallizing, Sept Iles melts. Temperatures below 850°C could represent sub-solidus temperatures that are recorded due to sub-solidus re-equilibration of mafic phases containing fast-diffusing elements.

Open-system behaviour in super-solidus magmatic systems may include addition or loss of chemical components. One example includes the loss of a buoyant immiscible Si-rich liquid from the interstitial melt (Holness *et al.*, 2011; Humphreys, 2011; Namur *et al.*, 2012*a*; Namur & Humphreys, 2018), a process that is thought to have taken place in the floor cumulates of the Skaergaard intrusion once the temperature in partially solidified crystal mush fell below 1020°C (Holness *et al.*, 2011; Charlier & Grove, 2012; Hou *et al.*, 2017; 2018). A further example is provided by the mobility of either hydrous fluids (Koepke *et al.*, 2005*a*; *b*; 2014; Wolff *et al.*, 2013) or melts into incompletely solidified rocks: the latter is known as

reactive porous flow (e.g. Lissenberg *et al.*, 2013; Namur et al., 2013; Lissenberg & MacLeod, 2016).

Critically, the open-system behaviour in Sept Iles (and, by extension, in the Skaergaard, Bushveld, Duluth, and Panzhihua intrusions) resulted in the formation of symplectites. Although Lissenberg & MacLeod (2016) documented clinopyroxene-amphibole symplectites replacing original clinopyroxene as a consequence of reactive porous flow in oceanic gabbros, the most common microstructural record of reactive porous flow they recognized is evidence of plagioclase dissolution. Plagioclase records irregular dissolution fronts within crystals, marked by compositional zoning and fingering, whereas other grains lose all semblance of original shapes formed during primary growth. We observed no comparable evidence of dissolution in the Sept Iles cumulates except, perhaps, in MCU III where plagioclase crystals contain irregular patches that luminesce blue.

The formation of anhydrous ("Skaergaard-type") symplectites

The anhydrous symplectites of the Sept Iles intrusion (Types I-a, I-c, and some examples of Type II-a in which there are no hydrous phases in the rims) are essentially identical to those previously described from the Skaergaard intrusion (Holness *et al.*, 2011), with similar relationships between symplectite abundance and the primocryst assemblage. The striking similarities, both physically and chemically, between the anhydrous Sept Iles symplectites and those of the Skaergaard suggest a similar history, with reaction triggered between a residual Fe-rich conjugate and the surrounding primocrysts, following the loss of the buoyant Si-rich conjugate (Holness *et al.*, 2011; Humphreys, 2011; Namur *et al.*, 2012*a*). Support for this hypothesis is provided by our temperature estimates, which fall slightly below the temperature of the onset of immiscibility in ferrobasaltic systems (~1020°C; Charlier & Grove, 2012). At this temperature, experiments from Charlier & Grove (2012) show that the

Sept Iles magma splits into an Fe-rich immiscible melt (42 wt.% SiO_2, 21.4 wt.% FeO_t) and a Si-rich immiscible melt (60.4 wt.% SiO_2, 10.3 wt.% FeO_t). The compositions of the immiscible melts differ more widely with decreasing temperature. Modelling of the Sept Iles liquid line of descent indicates that immiscibility develops after ca. 50% of fractionation (Namur et al., 2012*a*). Assuming an initial porosity of the crystal mush of ca. 30% (Tegner *et al.*, 2009; Namur & Charlier, 2012) we can confidently assume that the Sept Iles crystal mush at the onset of immiscibility was still sufficiently permeable to permit the escape of the buoyant Si-rich melt. As proposed for Skaergaard by Holness *et al.* (2011), we believe that separation between the two immiscible melts may have led to reaction between early-crystallized plagioclase in the crystal mush (that crystallized from a single-phase melt prior to the development of immiscibility), and the remaining Fe-rich immiscible conjugate. We suggest that this reaction and the Fe-rich nature of the immiscible melt led to the crystallization of highly anorthitic plagioclase and the mafic minerals found in the symplectites.

To test the hypothesis that the Sept Iles anhydrous reactive symplectites were generated by reaction of the mush with interstitial liquid after preferential loss of one of the immiscible conjugates, the bulk compositions of the Sept Iles replacive symplectites (with the exception of oxy-symplectites) were compared with the compositions of Si-rich and Fe-rich immiscible conjugates, together with that of the homogeneous liquid prior to the onset of unmixing in Fig. 11a and b. It is clear that the bulk compositions of some symplectites can be reproduced by mixing an Fe-rich endmember (assumed to be the Fe-rich immiscible conjugate liquid) with a plagioclase component (obtained by dissolution of primocrysts) (Fig. 11a and 11b), consistent with the model of Holness *et al.* (2011). However, this mixing model does not work for all symplectite bulk compositions, nor for some elements such as CaO (Fig. 11a). In addition, when plotted on a ternary diagram, and compared to the Sept Iles liquid line of

descent from Charlier & Grove (2012), the bulk compositions of the symplectites all fall in the one-liquid field, regardless of the symplectite type (Fig. 11c).

We therefore suggest the symplectites are to some extent the products of fractional crystallization in which the Fe-rich interstitial melt remaining after the loss of the Si-rich conjugate dissolved plagioclase to form a hybrid melt which then ultimately crystallized to form the symplectite, undergoing fractionation as it did so. Such a process is consistent with the progressive reduction of pyroxene Mg# and olivine Fo-content with crystallization in symplectite vermicules. Accordingly, the variability in symplectite bulk compositions represents the ratio of two components of the hybrid melt (dissolved plagioclase primocrysts and the Fe-rich conjugate liquid). This hypothesis explains why symplectite compositions plot on straight lines in CaO vs. FeO (Fig. 11a) and FeO vs. Al_2O_3 (Fig. 11b) diagrams.

In order to explain the highly anorthitic nature of the plagioclase found in the Skaergaard symplectites, it was proposed that the symplectite-forming reaction involves dissolution of mafic phases in addition to plagioclase (Holness *et al.*, 2011). In contrast, there is no petrographic evidence that minerals other than plagioclase dissolved prior to the crystallization of the Sept Iles symplectites, and we argue that crystallization of anorthitic symplectic plagioclase (resulting in bulk symplectite compositions with > 12 wt.% CaO) does not require dissolution of a mafic phase. Indeed, dissolution of primocryst plagioclase from a mafic magma leads to an increasing melt CaO/Na_2O ratio, which would therefore be in equilibrium with a progressively more anorthitic plagioclase.

Assuming symplectites formed from a hybrid liquid comprising the Fe-rich conjugate and a dissolved plagioclase component, we calculated the plagioclase composition expected to crystallize from this liquid, using the thermodynamic model of Namur *et al.* (2012*b*). We assumed the Fe-rich conjugate had the composition suggested by Charlier & Grove (2012)

and iteratively added increasing amounts of plagioclase An_{60} component, typical of the primocrysts. Accordingly, a hybrid liquid comprising ~50% dissolved plagioclase and ~50% Fe-rich immiscible melt would crystallize plagioclase of An_{90}, typical of that in reactive symplectites. Such dissolution would have no effect on the composition of associated mafic minerals, consistent with the observations in the Sept Iles intrusion.

The formation of Type I-b symplectites

We tentatively suggest that Type I-b symplectites are also related to this group of anhydrous symplectites: the amphibole vermicules in this rare group are replaced by pyroxene along their growth direction, and their location in the most evolved parts of the MCU II stratigraphy (pomica-C) is consistent with localized growth of amphibole instead of the more common pyroxene due to relatively high water contents of the interstitial liquid. Namur *et al.* (2011*a*) estimated that the melt in equilibrium with pomica-C cumulates that formed after ~50% of fractional crystallization of the Sept Iles parental magma may contain > 1.0-1.5 wt.% H_2O. This melt was only slightly more primitive than the amphibole-bearing rhyolitic melt that formed the Upper Zone and that resulted from ~60-70% of fractional crystallization of the parental magma.

Symplectite-free stratigraphy at the top of MCU II

Interestingly, near the top of the S-9 drill core at the top of MCU II there is ~50 m of stratigraphy apparently containing no symplectites at all, despite tight sample spacing (Fig. 5). In the Skaergaard intrusion, replacive symplectites related to liquid immiscibility are absent in cumulates containing pockets of granophyre. This anti-correlation provides a strong argument in support of the hypothesis that symplectite growth was triggered by the loss of an Si-rich immiscible conjugate: when such loss did not occur, the trapped Si-rich conjugate crystallized

as granophyre whereas the Fe-rich conjugate formed corresponding ilmenite-rich intergrowths (Holness *et al.*, 2011). However, such paired intergrowths are not present in the Sept Iles stratigraphy and granophyres are absent in the upper part of MCU II – we cannot therefore appeal to the retention of Si-rich liquid in the mush to explain the absence of symplectites at the top of MCU II.

Instead, the absence of symplectites in the pomica-C unit at the top of MCU II, which represents the most evolved cumulates observed in Sept Iles, may be because this is the only part of the stratigraphy that crystallized directly from immiscible melts (Charlier *et al.*, 2011; Namur *et al.*, 2012*a*). During crystallization of this unit, the main magma body developed immiscibility. In contrast, in all other parts of the stratigraphy, immiscibility developed only in the crystal mush after extensive crystallization of the interstitial melt. The effect is that the two immiscible conjugates in the pomica-C unit at the top of MCU II continuously maintained chemical communication during solidification, preventing the initiation of symplectite-forming reactions. Charlier *et al.* (2011) argued that the two immiscible conjugates formed alternating melt layers on a scale of only 50 cm to 1 m, which remained in physical contact and therefore also in thermodynamic equilibrium. As a consequence, no reactions were triggered by the breakdown of chemical equilibrium consequent to the loss of Si-rich melt. This means that primocrysts with identical compositions are present in layers crystallized dominantly from either the Fe-rich melt or the Si-rich melt because these two melts had similar activities of chemical components. However, crystallization of these two melts led to the formation of melanocratic layers (the crystallization product of the Fe-rich conjugate) alternating with leucocratic layers (the crystallization product of the Si-rich conjugate) on a scale of only 50 cm to 1 m.

Summary of Immiscibility Model

The formation of Types I-a, I-c, likely I-b, and some II-a symplectites by separation of conjugate immiscible melts provides an explanation for the relative scarcity of these symplectites in MCU I, where immiscibility was most likely of minor importance, compared to MCU II and/or MCU III where immiscibility developed in the bulk magma (Namur *et al.*, 2012*a*). This also explains the complete absence of symplectites in the upper part of MCU II in which cumulates crystallized from unmixed melts (Namur *et al.*, 2012*a*). The development of immiscibility in the main magma body of MCU II (and probably MCU III) and the absence of large-scale immiscibility during the crystallization of MCU I is related to the different parental magma compositions of the various megacyclic units. As shown by Namur *et al.* (2012*a*), magma mixing between primitive melt and resident melt from MCU I formed the parental melt composition of MCU II, which by differentiation entered the two-liquid field experimentally determined by Charlier & Grove (2012). In contrast, the melts from MCU I never entered this field, partly because they are slightly poorer in elements enlarging the two-liquid field (e.g. P_2O_5, $Na_2O + K_2O$) but also because the magma chamber was replenished before the melts of MCU I became highly differentiated (Namur *et al.*, 2010; 2012*a*).

As suggested above, the formation of highly anorthitic plagioclase in symplectites is due to reactive dissolution of plagioclase primocrysts by an Fe-rich immiscible melt followed by reprecipitation (Fig. 12). This reaction takes place during, or just after, gravitational loss of the conjugate Si-rich melt and is a result of the very different CaO/Na_2O ratios in the two conjugate liquids and also in the homogeneous melt that crystallized the plagioclase primocrysts. In contrast, the Mg# of the symplectite mafic phases is relatively similar to that of the primocrysts. As an example, symplectites containing clinopyroxene in evolved cumulates from MCU II have a Mg# (60-70) identical to the primocrysts in the same samples (Fig. 9b). Note that the most primitive symplectite clinopyroxene (Mg# > 75) occurs in samples that do not contain clinopyroxene primocrysts (see above). In a similar way, olivine

in symplectites has a low Fo-content (35-45), identical to the Fo-content of primocrysts in pomica-C samples containing olivine-bearing symplectites. The relatively similar Mg# (or Fo) between symplectites and primocrysts is explained by both the conjugate immiscible melts having almost identical Mg# (Charlier & Grove, 2012) and by the absence of significant evolution of the composition of mafic minerals throughout the Sept Iles stratigraphy, except in apatite-bearing cumulates (Namur *et al.,* 2010). As a consequence, the loss of the Si-rich melt from the crystal mush does not create significant chemical disequilibrium between the primocrysts and the Fe-rich melt; the parental melt to the symplectites thus crystallize mafic rims and vermicules of a composition similar to that of the primocrysts. Even where dissolution of the mafic phases following the loss of the Si-rich conjugate is only minor, mafic rims and vermicules in the symplectites would still have a composition identical to that of the olivine and pyroxene primocrysts.

The formation of hydrous symplectites in the Sept Iles intrusion

Type II-b, biotite-plagioclase symplectites, and Type II-a symplectites that contain hydrous phases, are unlike any symplectites seen in the Skaergaard intrusion in that they contain a much larger fraction of hydrous minerals than any Skaergaard symplectites. The origin of these symplectites is unclear. Although they could originate via a process of differential loss of immiscible liquids similar to that proposed for hydrous symplectites (e.g. Wang *et al.*, 2018), they are much more H_2O-rich than the dry, biotite-free, pomica-C cumulates crystallized from immiscible melts (Charlier *et al,* 2011; Namur *et al.,* 2012*a*). This means that the symplectites have formed from a melt containing more water than either of the immiscible conjugates. As shown by Charlier *et al.* (2011) and Charlier & Grove 2012), the immiscible melts are only slightly more primitive (Mg# 15-20) than the residual rhyolitic melt (Mg# 5-22; Namur *et al.*, 2011*a*) following fractionation of the pomica-C cumulates.

Crystallization of these rocks drove the bulk liquid composition outside the two-liquid field and produced a rhyolite that ultimately formed the amphibole-rich granite of the Upper Zone. However, as shown by the pomica-C cumulates, the crystallization product of the immiscible melts (pomica-C cumulates) is dry, illustrating that the immiscible melts were never in equilibrium with hydrous phases. We therefore believe that a process other than reaction between plagioclase primocrysts and an Fe-rich immiscible liquid is needed to explain the formation of Type II-b and biotite-plagioclase symplectites.

Natural and experimental studies on oceanic gabbros offer an alternative explanation for the origin of hydrous symplectites (Koepke *et al.*, 2004; 2005*a*; 2005*b*; 2014; Wolff *et al.*, 2013). It has been proposed that hydrous symplectites can be generated during partial melting reactions triggered by pervasive infiltration of hydrous fluids. Following this model, mafic phases (olivine, pyroxene) and moderately anorthitic plagioclase react with a water-dominated fluid to form pyroxene, amphibole, and highly anorthitic plagioclase. Several aspects of Type II-b (as well as perhaps I-b and some II-a) symplectites suggest that a process comparable, but not identical, to hydrous partial melting may have contributed to their formation.

One of the major arguments for the mobility of reactive fluids in the Sept Iles cumulates is provided by cathodoluminescence imaging of plagioclase-plagioclase grain boundaries that luminesce bright green, in contrast to the blue luminescence of the centres of the plagioclase primocrysts. We thus suggest that anorthitic plagioclase rims formed as a result of hydrous fluid circulation. However, the process and reactions proposed by Koepke *et al.* (2004) do not fully account for Sept Iles symplectites in which only plagioclase was replaced.

Instead, we propose that hydration occurred under super-solidus conditions, when exsolution of a hydrous volatile phase from deeper parts of the mush led to the migration of a free fluid phase in the upper part of the mush, perhaps accompanied by migration of a fluid-saturated

melt. This led to significant plagioclase dissolution and the re-crystallization of more anorthitic plagioclase due to an increase of the CaO/Na_2O ratio of the interstitial liquid. Some of the fluid phase may also have re-dissolved in the drier interstitial melt in the upper part of the fluid, resulting in an increase in water activity and the stabilization of highly anorthitic plagioclase (Lange *et al.*, 2009). Where there was sufficient interstitial melt to permit convection within the mush, much more extensive plagioclase dissolution may have occurred, as shown in Fig. 8b, where only small amounts of blue relic plagioclase primocrysts are observed. We suggest that melt circulation, resulting in mixing between fluid-saturated melt from the deepest part of the mush and fluid-undersaturated melt in the upper part of the mush, may explain why amphibole vermicules of some Type II-b symplectites grade outward into pyroxene along the growth direction. Hornblende-plagioclase thermometry suggests the Sept Iles Type II-b symplectites formed at ~800-1000°C, consistent with the temperature of formation of water-saturated evolved residual rhyolitic melts (e.g. Bogaerts *et al.*, 2006).

Although fluid exsolution from deeper in the mush is the most likely source for hydrous fluids, other sources cannot be excluded. In the Sept Iles Layered Series, symplectites containing hydrous minerals occur in the upper parts of MCU II and are particularly abundant throughout MCU III. Near-surface alteration from meteoric water, infiltrating either along a system of fractures or along high-temperature shear zones (Koepke *et al.*, 2014), could potentially account for the abundance of hydrous symplectites throughout MCU III, as well as the pervasive green luminescence of the plagioclase crystals. The Sept Iles Layered Series also contains many anorthositic fallen roof blocks (Namur *et al.*, 2011*b*). Many such blocks contain evidence for hydrothermal alteration and, if some of this fluid were released after the blocks arrived on the intrusion floor, this could provide water to trigger melting reactions. A general model of the symplectite-forming process, involving dissolution-precipitation reactions, is shown in Fig. 13.

CONCLUSIONS

We have documented and classified seven different symplectite types in the Sept Iles intrusion, most of them replacing plagioclase. Oxy-symplectites resulted from oxygen fugacity differences in the residual liquid. Types I-a, I-c, and many Type II-a symplectites, are identical to those described in the Skaergaard intrusion (Holness *et al.*, 2011): these are dominant in MCU II where the evolved bulk liquid entered the two-liquid stability field, and likely formed by reaction triggered by the differential loss of an unmixed Si-rich immiscible conjugate from the crystal mush. Type I-b symplectites contain amphibole, but their similarities to Type I-c symplectites suggest that they might also be connected to differential migration of immiscible interstitial liquids. Reaction occurred because the two immiscible conjugates have highly contrasted CaO/Na_2O ratios which are also different from the CaO/Na_2O ratio of the melt that crystallized plagioclase primocrysts. When immiscible melts are segregated, the Fe-rich melt that stays in the mush is in strong chemical disequilibrium with plagioclase primocrysts. This leads to plagioclase dissolution followed by reprecipitation, accounting for the highly anorthitic nature of the plagioclase in these symplectites.

Type II-b and the biotite-plagioclase symplectites, as well as the Type II-a symplectites with hydrous phases, differ from those of the Skaergaard intrusion. Their hydrous nature and similarities with microstructures formed during hydrous partial melting experiments suggest that these types of symplectite may be related to the infiltration of hydrous fluids in the super-solidus regime. We suggest that exsolution of volatiles from highly evolved melt increases the water activity of the intercumulus melt in the overlying mush, leading to the dissolution of plagioclase primocrysts and re-precipitation of anorthitic symplectite plagioclase. Such a

process also formed anorthitic rims on some plagioclase crystals. The abundance of hydrous symplectites in MCU III, where the most hydrothermal circulation has occurred, is consistent with this hypothesis.

All replacive symplectites in the Sept Iles formed from dissolution-precipitation reactions rather than by diffusion. As replacive symplectites are ubiquitous features in layered mafic intrusions, similar petrographic and compositional work on symplectites in different mafic intrusions can further refine the hypotheses developed in this study.

FUNDING

This project formed part of a Master's thesis completed by HAK at the University of Cambridge. HAK was funded by the Bill and Melinda Gates Foundation on a Gates Cambridge Scholarship. ON gratefully acknowledges support from Magdalene College, University of Cambridge, and the FWO for the Odysseus grant.

ACKNOWLEDGEMENTS

We are grateful to Tony Dickson, Iris Buisman, and Giulio Lampronti for advice and help with the cathodoluminescence microscope, microprobe, and scanning electron microscope, respectively.

REFERENCES

Andersen, D.J., Lindsley, D.H., & Davidson, P.M. (1993). QUILF: A Pascal program to assess equilibria among Fe-Mg-Mn-Ti oxides, pyroxenes, olivine, and quartz. *Computers and Geosciences* **19**, 1333-1350.

Ashwal, L.D., Webb, S.J., & Knoper, M.W. (2005). Magmatic stratigraphy in the Bushveld Northern Lobe: continuous geophysical and mineralogical data from the 2950 m Bellevue drillcore. *South African Journal of Geology* **108**, 199-232

Bachmann, O., & Huber, C. (2016). Silicic magma reservoirs in the Earth's crust. *American Mineralogist* **101**, 2377-2404.

Barnes, S.J., Le Vaillant, M., & Lightfoot, P.C. (2017). Textural development in sulfide-matrix ore breccias in the Voisey's Bay Ni-Cu-Co deposit, Labrador, Canada. *Ore Geology Reviews* **90**, 414-438.

Bogaerts, M., Scaillet, B., & Vander Auwera, J. (2006). Phase equilibria of the Lyngdal granodiorite (Norway): Implications for the origin of metaluminous ferroan granitoids. *Journal of Petrology* **47**, 2405-2431.

Boudreau, A.E., & McCallum, I.S. (1989). Investigations of the Stillwater Complex: Part V. Apatites as indicators of evolving fluid composition. *Contributions to Mineralogy and Petrology* **102**, 138-153.

Boudreau, A.E., Mathez, E.A., & McCallum, I.S. (1986). Halogen geochemistry of the Stillwater and Bushveld Complexes: Evidence for transport of the platinum-group elements by Cl-Rich fluids. *Journal of Petrology* **27**, 967-986.

Cashman, K.V., Sparks, R.S.J., & Blundy, J.D. (2017). Vertically extensive and unstable magmatic systems: a unified view of igneous processes. *Science* **355**, 6331.

Charlier, B., & Grove, T.L. (2012). Experiments on liquid immiscibility along tholeiitic liquid lines of descent. *Contributions to Mineralogy and Petrology* **164**, 27-44.

Charlier, B., Namur, O., Toplis, M.J., Schiano, P., Cluzel, N., Higgins, M.D., & Vander Auwera, J. (2011). Large-scale silicate liquid immiscibility during differentiation of tholeiitic basalt to granite and the origin of the Daly gap. *Geology* **39**, 907-910.

Charlier, B., Namur, O., & Grove, T.L. (2013). Compositional and kinetic controls on liquid immiscibility in ferrobasalt–rhyolite volcanic and plutonic series. *Geochimica et Cosmochimica Acta* **113**, 79-93.

Cimon, J. (1998). *Le Complexe de Sept-Îles: I-L'Unité à apatite de Rivière des Rapides, Complexe de Sept-Îles; localisation stratigraphique et facteurs à l'origine de sa formation.* Québec: Ministère de l'Energie et des Ressources du Québec, pp. 1-33.

Efimov, A.A., & Malitch, K.N. (2012). Magnetite-orthopyroxene symplectites in gabbros of the Urals: A structural track of olivine oxidation. *Geology of Ore Deposits* **54**, 531-539.

Fischer, L.A., Wang, M., Charlier, B., Namur, O., Roberts, R.J., Veksley, I.V., & Holtz, F. (2016). Immiscible iron- and silica-rich liquids in the Upper Zone of the Bushveld Complex. *Earth and Planetary Science Letters* **443**, 108-117.

Gál, B., Molnár, F., & Peterson, D.M. (2011). Cu-Nu-PGE mineralization in the South Filson Creek area, South Kawishiwi Intrusion, Duluth Complex: mineralization styles and magmatic and hydrothermal processes. *Economic Geology* **106**, 481-509.

Henry, D.J., Guidotti, C.V., & Thomson, J.A. (2005). The Ti-saturation surface for low-to-medium pressure metapelitic biotites: implications for geothermometry and Ti-substitution mechanisms. *American Mineralogist*, **90**, 316-328.

Higgins, M.D. (2005). A new model for the structure of the Sept Iles Intrusive suite, Canada. *Lithos* **83**, 199-213.

Higgins, M.D., & Doig, R. (1981). The Sept Iles anorthosite complex: Field relationships, geochronology and petrology. *Canadian Journal of Earth Sciences* **18**, 561-573

Higgins, M.D., & van Breemen, O. (1998). The age of the Sept Iles layered mafic intrusion, Canada: Implications for the Late Neoproterozoic/Cambrian history of Southeastern Canada. *Journal of Geology* **106**, 421-431.

Holland, T., & Blundy, J. (1994). Non-ideal interactions in calcic amphiboles and their bearing on amphibole-plagioclase thermometry. *Contributions to Mineralogy and Petrology* **116**, 433-447.

Holness, M.B., Stripp, G., Humphreys, M.C.S., Veksler, I.V., Nielsen, T.F.D., & Tegner, C. (2011). Silicate liquid immiscibility within the crystal mush: Late-stage magmatic microstructures in the Skaergaard intrusion, East Greenland. *Journal of Petrology* **52**, 175-222.

Holness, M.B., Tegner, C., Nielsen, T.F.D., & Charlier, B. (2017).The thickness of the mushy layer on the floor of the Skaergaard magma chamber at apatite saturation. *Journal of Petrology* **58**, 909-932.

Hou, T., Charlier, B., Namur, O., Schütte, P., Schwarz-Schampera, U., Zhang, Z., Holtz, F. (2017). Experimental study of liquid immiscibility in the Kiruna-type Vergenoeg iron-fluorine deposit, South Africa. Geochimica et Cosmochimica Acta **203**, 303-322.

Hou, T., Charlier, B., Holtz, F., Veksler, I., Zhang, Z., Thomas, R., Namur, O. (2018). Immiscible hydrous Fe-Ca-P melt and the origin of iron oxide-apatite ore deposits. Nature Communications **9**, 1415.

Huber, C., Bachmann, O., & Manga, M. (2010). Two competing effects of volatiles on heat transfer in crystal-rich magmas: thermal insulation vs. defrosting. *Journal of Petrology* **51**, 847-867.

Humphreys, M.C.S. (2009). Chemical evolution of intercumulus liquid, as recorded in plagioclase overgrowth rims from the Skaergaard Intrusion. *Journal of Petrology* **50**, 127-145.

Humphreys, M.C.S. (2011). Silicate liquid immiscibility within the crystal mush: Evidence from Ti in plagioclase from the Skaergaard Intrusion. *Journal of Petrology* **52**, 147-174.

Ikeda, T., Nishiyama, T., Yamada, S., & Yanagi, T. (2007). Microstructures of olivine-plagioclase corona in meta-ultramafic rocks from Sefuri Mountains, NW Kyushu, Japan. *Lithos* **97**, 289-306.

Irvine, T.N. (1980). *Magmatic infiltration metasomatism, double-diffusive fractional crystallization, and adcumulus growth in the Muskox Intrusion and other layered intrusions*. In: Hargrave, R.B. (ed.) Physics of magmatic processes. Princeton University Press, 325-383.

Irvine, T.N. (1982). Terminology for layered intrusions. *Journal of Petrology* **95**, 451-461.

Jakobsen, J.K., Veksler, I. Tegner, C., & Brooks, C.K. (2005). Immiscible iron- and silica-rich melts in basalt petrogenesis documented in the Skaergaard intrusion. Geology **33**, 885-888.

Kent, A.J., Darr, C., Koleszar, A.M., Salisbury, M.J., & Cooper, K.M. (2010). Preferential eruption of andesitic magmas through recharge filtering. *Nature Geoscience* **3**, 631-636.

Koepke, J., Feig, S.T., Snow, J., & Freise, M. (2004). Petrogenesis of oceanic plagiogranites by partial melting of gabbros: an experimental study. *Contributions to Mineralogy and Petrology* **146**, 414-432.

Koepke, J., Feig, S.T., & Snow, J. (2005*a*). Late-stage magmatic evolution of oceanic gabbros as a result of hydrous partial melting: Evidence from the ODP Leg 153 drilling at the Mid-Atlantic Ridge. *Geochemistry, Geophysics, Geosystems* **6**, 1-27.

Koepke, J., Feig, S.T., & Snow, J. (2005*b*). Hydrous partial melting in the lower oceanic crust. *Terra Nova* **17**, 286-291.

Koepke, J., Berndt, J., Horn, I., Fahle, J., & Wolff, P.E. (2014). Partial melting of oceanic gabbro triggered by migrating water-rich fluids: a prime example from the Oman ophiolite. *Geological Society, London, Special Publications* **392**, 195-212.

Kumarapeli, P.S., & Saull, V.A. (1966). The St. Lawrence Valley system: A North American equivalent of the East African rift system. *Canadian Journal of Earth Sciences* **3**, 639-657.

Lange, R.A., Frey, H.M., & Hector, J. (2009). A thermodynamic model for the plagioclase-liquid hygrometer/thermometer. *American Mineralogist* **94**, 494-506.

Leuthold, J., Blundy, J.D., Holness, M.B., & Sides, R. (2014). Successive episodes of reactive liquid flow through a layered intrusion (Unit 9, Rum Eastern Layered Intrusion, Scotlan). *Contributions to Mineralogy and Petrology* **168**, 1-27.

Lissenberg, C.J., & MacLeod, C.J. (2016). A reactive porous flow control on mid-ocean ridge magmatic evolution. *Journal of Petrology* **57**, 2195-2220.

Lissenberg, C.J., MacLeod, C.J., Howard, K.A., & Godard, M. (2013). Pervasive reactive melt migration through fast-spreading lower oceanic crust (Hess Deep, equatorial Pacific Ocean). *Earth and Planetary Science Letters* **361**, 436-447.

Loncarevic, B.D., Feininger, T., & Lefebvre, D. (1990). The Sept Iles layered mafic intrusion: Geophysical expression. *Canadian Journal of Earth Sciences* **27**, 501-512.

McBirney, A.R. (1996). *The Skaergaard intrusion.* In: Cawthorn, R.G. (Ed.) Layered Intrusions. Amsterdam, Elsevier, 147-180.

Meurer, W.P., & Meurer, M.E.S. (2006). Using apatite to dispel the "trapped liquid" concept and to understand the loss of interstitial liquid by compaction in mafic cumulates: an example from the Stillwater Complex, Montana. *Contributions to Mineralogy and Petrology* **151**, 187-201.

Meurer, W.P., Klaber, S., & Boudreau, A.E. (1997). Discordant bodies from olivine-bearing zones III and IV of the Stillwater Complex, Montana: Evidence for postcumulus fluid migration and reaction in layered intrusions. *Contributions to Mineralogy and Petrology*, **130**, 81-92.

Morse, S.A., & Nolan, K.M. (1984). Origin of strongly reversed rims on plagioclase in cumulates. *Earth and Planetary Science Letters* **68**, 485-498.

Moseley, D. (1984). Symplectic exsolution in olivine. *American Mineralogist* **69**, 139-153.

Namur, O., & Charlier, B. (2012). Efficiency of compaction and compositional convection during mafic crystal mush solidification: the Sept Iles layered intrusion, Canada. *Contributions to Mineralogy and Petrology* **163**, 1049-1068.

Namur, O., & Humphreys, M.C.S. (2018). Trace element constraints on the differentiation and crystal mush solidification in the Skaergaard intrusion, Greenland. *Journal of Petrology* **59**, 387-418.

Namur, O., Hatert, F., Grandjean, F., Long, G.J., Krins, N., Fransolet, A., Vander Auwera, J., & Charlier, B. (2009). Ti substitution mechanisms in phlogopites from the Suwalki massif-type anorthosite, NE Poland. *European Journal of Mineralogy* **21**, 397-406.

Namur, O., Charlier, B., Toplis, M.J., Higgins, M.D., Liégeois, J., & Vander Auwera, J. (2010). Crystallization sequence and magma chamber processes in the ferrobasaltic Sept Iles Layered Intrusion, Canada. *Journal of Petrology* **51**, 1203-1236.

Namur, O., Charlier, B., Toplis, M.J., Higgins, M.D., Hounsell, V., Liégeois, J.P., & Vander Auwera, J. (2011*a*). Differentiation of tholeiitic basalt to A-type granite in the Sept Iles layered intrusion, Canada. *Journal of Petrology* **52**, 487-539.

Namur, O., Charlier, B., Pirard, C., Hermann, J., Liégeiusm J., & Vander Auwera, J. (2011*b*). Anorthosite formation by plagioclase flotation in ferrobasalt and implications for the lunar crust. *Geochimica et Cosmochimica Acta* **75**, 4998-5018.

Namur, O., Charlier, B., & Holness, M.B. (2012*a*). Dual origin of Fe-Ti-P gabbros by immiscibility and fractional crystallization of evolved tholeiitic basalts in the Sept Iles layered intrusion. *Lithos* **154**, 100-114.

Namur, O., Charlier, B., Toplis, M.J., & Vander Auwera, J. (2012*b*). Prediction of plagioclase-melt equilibria in anhydrous silicate melts at 1-atm. *Contributions to Mineralogy and Petrology* **163**, 133-150.

Namur, O., Humphreys, M.C.S., & Holness, M.B. (2013). Lateral reactive infiltration in a vertical gabbroic crystal mush, Skaergaard intrusion, East Greenland. *Journal of Petrology* **54**, 985-1016.

Namur, O., Humphreys, M.C.S., & Holness, M.B. (2014). Crystallization of interstitial liquid and latent heat buffering in solidifying gabbros: Skaergaard intrusion, Greenland. *Journal of Petrology* **55**, 1389-1427.

Namur, O., Higgins, M., & Vander Auwera, J. (2015). *The Sept Iles Intrusive Suite, Quebec, Canada.* In: Charlier, B., Namur, O., Latypov, R., & Tegner, C. (Eds.) Layered Intrusions. Springer Geology, 465-515.

Neave, D.A., Maclennan, J., Hartley, M.E., Edmonds, M., & Thordarson, T. (2014). Crystal storage and transfer in basaltic systems: the Skuggafjöll eruption, Iceland. *Journal of Petrology* **55**, 2311-2346.

Passmore, E., Maclennan, J., Fitton, G., & Thodarson, T. (2012). Mush disaggregation in basaltic magma chambers: evidence from the AD 1783 Laki eruption. *Journal of Petrology* **53**, 2593-2623.

Pitra, P., & de Waal, S.A. (2001). High-temperature, low-pressure metamorphism and development of prograde symplectites, Marble Hall Fragment, Bushveld Complex (South Africa). *Journal of Metamorphic Geology* **19**, 311-325.

Putirka, K.D. (2008). Thermometers and barometers from volcanic systems. In: Putirka, K.D., Tepley, F.J. (Eds.), Minerals inclusions and volcanic processes. *Reviews in Mineralogy and Petrology* **69**, 61-120.

Putnis, A., & Austrheim, H. (2010). Fluid-induced processes: metasomatism and metamorphism. *Geofluids* **10**, 244-269.

Roelofse, F., & Ashwal, L.D. (2008). Symplectic augite from the Platreef – textural evidence for fluid/rock interaction in the Northern Sector of the Northern Limb of the Bushveld Complex? *South African Journal of Geology* **111**, 21-26.

Roelofse, F., Ashwal, L.D., Pineda-Vargas, C.A., & Przybylowicz, W.J. (2009). Enigmatic textures developed along plagioclase-augite grain boundaries at the base of the Main Zone, Northern Limb, Bushveld Complex – evidence for late stage melt infiltration into a nearly solidified crystal mush. *South African Journal of Geology* **112**, 39-46.

Scott, J.M., Konrad-Schmolke, M., O'Brien, P.J., & Günter, C. (2013). High-T, Low-P formation of rare olivine-bearing symplectites in Variscan eclogite. *Journal of Petrology* **54**, 1375-1398.

Spruzeniece, L., Piazolo, S., Daczko, N.R., Kilburn, M.R., & Putnis, A. (2017). Symplectite formation in the presence of a reactive fluid: insights from hydrothermal experiments. *Journal of Metamorphic Geology* **35**, 281-299.

Tanner, D., Mavrogenes, J.A., Arculus, R.J., & Jenner, F.E. (2014). Trace element stratigraphy of the Bellevue Core, Northern Bushveld: Multiple magma injections obscured by diffusive processes. *Journal of Petrology* **55**, 859-882.

Tegner, C., Thy, P., Holness, M.B., Jakobsen, J.K., & Lesher, C.R. (2009). Differentiation and Compaction in the Skaergaard Intrusion. *Journal of Petrology* **50**, 813-840.

Thy, P., Lesher, C.E., Nielsen, T.F., & Brooks, C.K. (2006). Experimental constraints on the Skaergaard liquid line of descent. *Lithos* **92**, 154-180.

Thy, P., Tegner, C., & Lesher, C.E. (2009). Liquidus temperatures of the Skaergaard magma. *American Mineralogist* **94**, 1371-1376.

Toplis, M.J., & Carroll, M.R. (1995). An experimental study of the influence of oxygen fugacity on Fe-Ti oxide stability, phase relations, and mineral-melt equilibria in ferro-basaltic systems. *Journal of Petrology* **36**, 1137-1170.

Turner, S.P., & Stüwe, K. (1992). Low-pressure corona textures between olivine and plagioclase in un-metamorphosed gabbros from Black Hill, South Australia. *Mineralogical Magazine* **56**, 503-509.

Wang, K., Wang, C.Y., & Ren, Z.Y. (2018). Apatite-hosted melt inclusions from the Panzhihua gabbroic-layered intrusion associated with a giant Fe–Ti oxide deposit in SW China: insights for magma unmixing within a crystal mush. *Contributions to Mineralogy and Petrology* **173:59**.

Wolff, P.E., Koepke, J., & Feig, S.T. (2013). The reaction mechanism of fluid-induced partial melting of gabbros in the oceanic crust. *European Journal of Mineralogy* **25**, 279-298.

Xie, Q., Zhang, Z., Cheng, Z., & Santosh, M. (2017). Interstitial microstructures in Ji'nan mafic intrusion, North China Craton: magmatic or hydrothermal origin? *European Journal of Mineralogy* **29**, 839-850.

Yang, A.Y., Wang, C., Liang, Y., & Lissenberg, C.J. (2019). Reaction between mid-ocean ridge basalt and lower oceanic crust: An experimental study. *Geochemistry, Geophysics, Geosystems* **20**, 4390-4407.

Yuan, Q., Namur, O., Fischer, L.A., Roberts, R.J., Lü, X., & Charlier, B. (2017). Pulses of plagioclase-laden magmas and stratigraphic evolution in the Upper Zone of the Bushveld Complex, South Africa. *Journal of Petrology* **58**, 1619-1643.

Table and Figure Captions

Table 1. Classification of the main symplectite categories in the Sept Iles Layered Series, based on the root primocryst and the compositions of the phases involved in the symplectite. Fe-Ti Oxide = magnetite ± ilmenite, Opx = orthopyroxene, Cpx = clinopyroxene.

Symplectite Type	Root Primocryst	Symplectite Composition
Type I	Fe-Ti Oxide	Anorthitic plagioclase with Opx (± Cpx/Amphibole/Olivine)
Type II	Olivine	Anorthitic plagioclase with Opx (± Cpx/Amphibole/Olivine)
Oxy-Symplectite	Olivine	Orthopyroxene with magnetite (± ilmenite)
Biotite-Plagioclase	Fe-Ti Oxide	Anorthitic plagioclase with biotite

Table 2. Minimum, maximum, and average temperatures produced from thermometry calculations on both symplectite and rim phases from the Sept Iles Layered Series.

Thermometer	Reference	Min. (°C)	Max. (° C)	Average (°C)
Amphibole-plagioclase for amphibole rims/plagioclase primocrysts	Holland & Blundy (1994)	737	932	852
Amphibole-plagioclase for symplectites	Holland & Blundy (1994)	784	1007	899
Clinopyroxene-orthopyroxene in symplectite using QUILF	Anderson *et al.* (1993)	751	892	821
Clinopyroxene-orthopyroxene in symplectite	Putirka (2008)	777	910	835
Ti content in biotite	Henry *et al.* (2005); Namur *et al.* (2009)	665	980	926

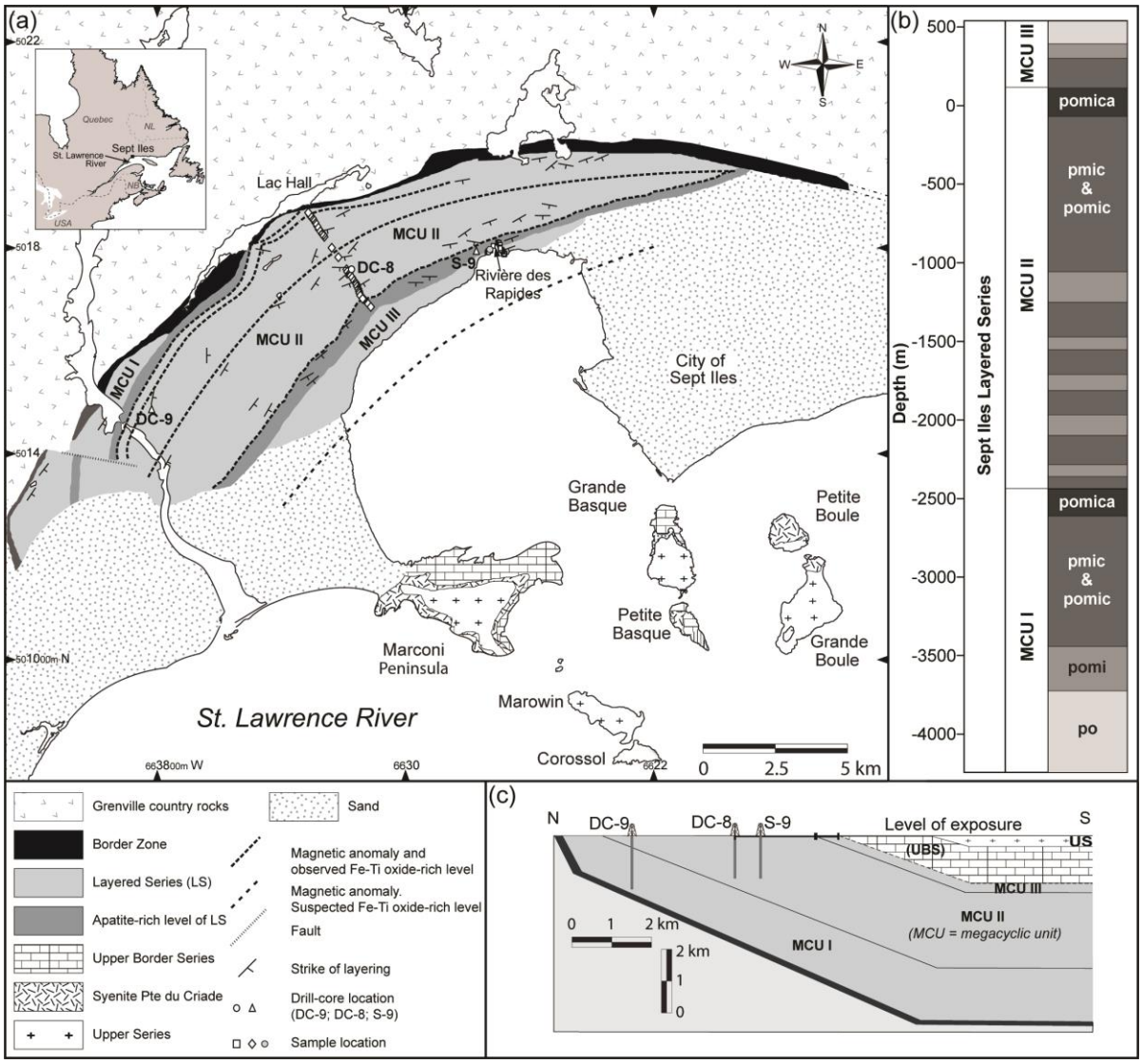

Fig. 1. a) Geologic map of the Sept Iles layered intrusion, showing the three megacyclic units MCU I, II, and III. Locations of drill holes DC-8, DC-9, and S-9 are shown, along with the locations of sample sites. Inset shows the location of the Sept Iles intrusion in eastern Canada. "US" = Upper Series; "UBS" = Upper Border Series." b) Stratigraphic section through all three megacyclic units of the Sept Iles layered intrusion (from Namur *et al.*, 2012*a*), showing the various rock types observed: troctolites = "po-C", Fe-Ti oxide-bearing troctolites = "pomi-C", gabbros = "pomic-C", "pmic-C", and apatite-bearing gabbros = "pomica-C", where p = plagioclase, o = olivine, m = magnetite, i = ilmenite, a = apatite, and C = cumulus. Classification from Irvine (1982). c) Schematic cross-section of part of the Sept Iles intrusion,

showing the location of the drill cores where samples were collected from. Note the ~30° dip of the margins of the intrusion towards the centre. Modified from Namur *et al.* (2010). Adapted from Higgins (2005).

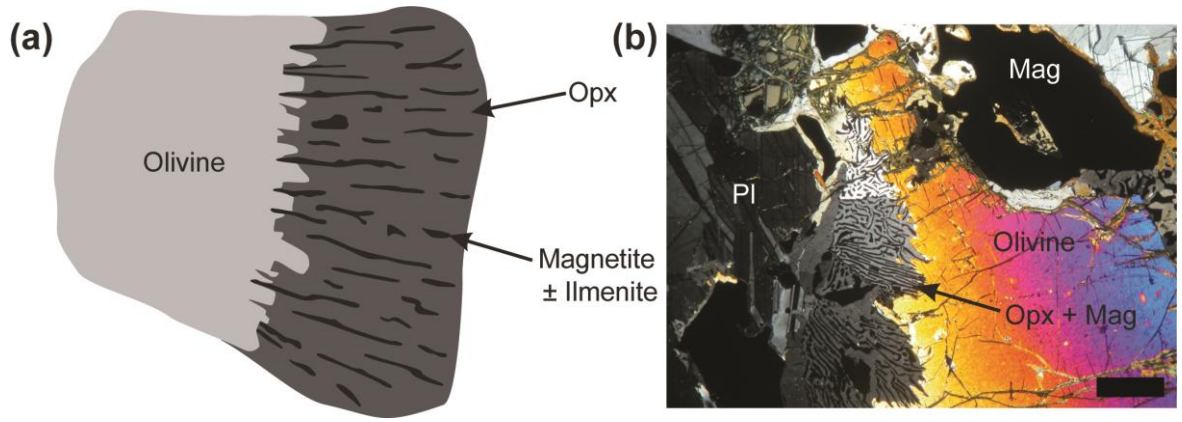

Fig. 2. a) Schematic diagram of an oxy-symplectite, showing orthopyroxene and Fe-Ti oxide vermicules replacing primocryst olivine. The vermicules in oxy-symplectites can be linear or curved. b) Crossed polarized photo micrograph of an oxy-symplectite from sample 8-439, MCU II. Pl = primocryst plagioclase, Opx = orthopyroxene, Mag = magnetite. Scale bar is 1 mm long.

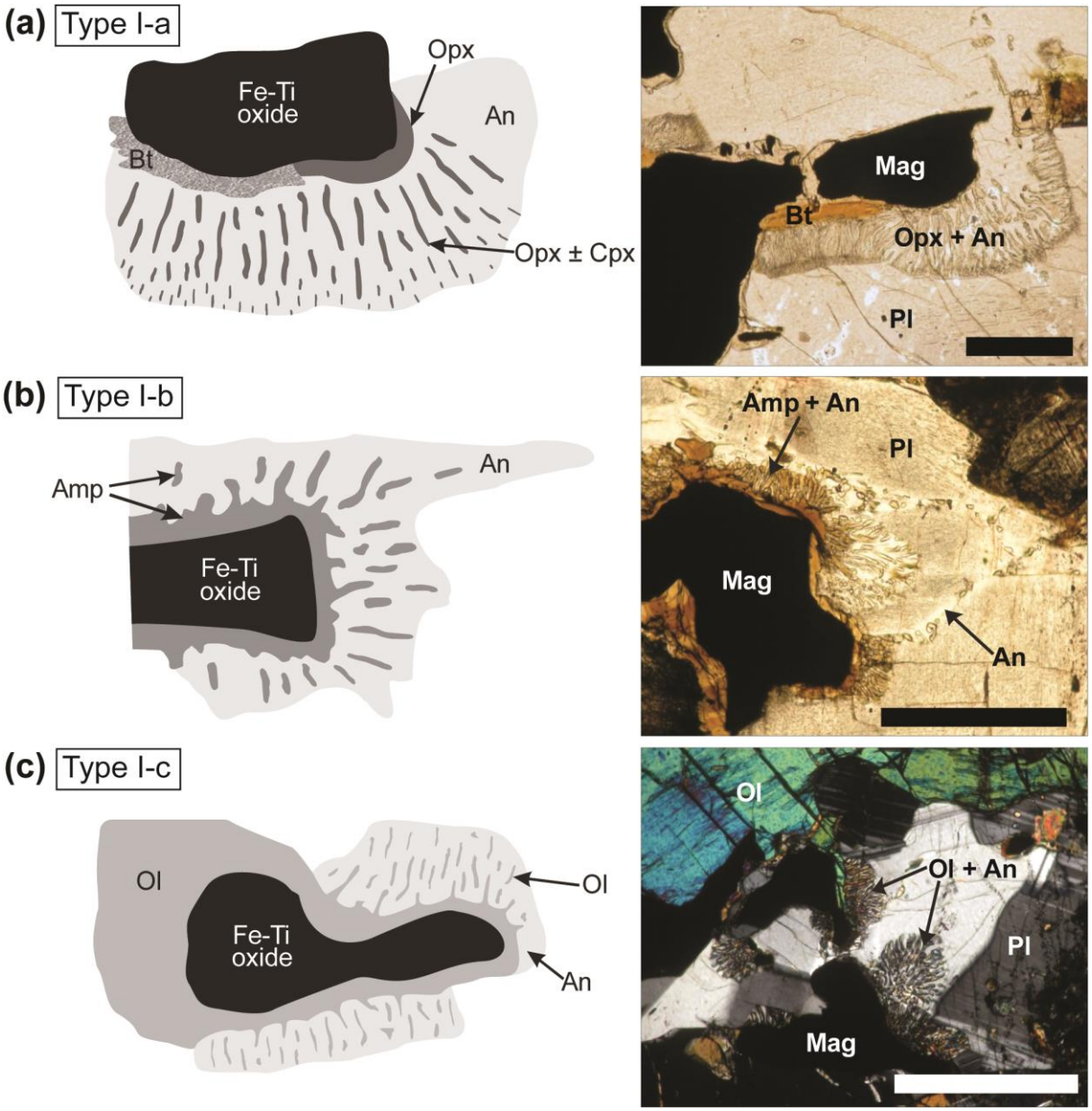

Fig. 3. a) Schematic diagram of a Type I-a symplectite (left), and plane polarized photo micrograph (right) of a typical Type I-a symplectite from sample 8-689, MCU II. b) Schematic diagram of a Type I-b symplectite (left), and plane polarized photo micrograph (right) of a typical Type I-b symplectite from sample ON-07-152, MCU II. c) Schematic diagram of a Type I-c symplectite (left), and crossed polarized photo micrograph (right) of a typical Type I-c symplectite from sample S9-33-3, MCU II. Fe-Ti Oxide = magnetite ± ilmenite, Mag = magnetite, Bt = biotite, Opx = orthopyroxene, Cpx = clinopyroxene, An =

anorthitic plagioclase, Pl = primocryst plagioclase, Amp = amphibole, Ol = olivine. All scale bars are 1 mm long.

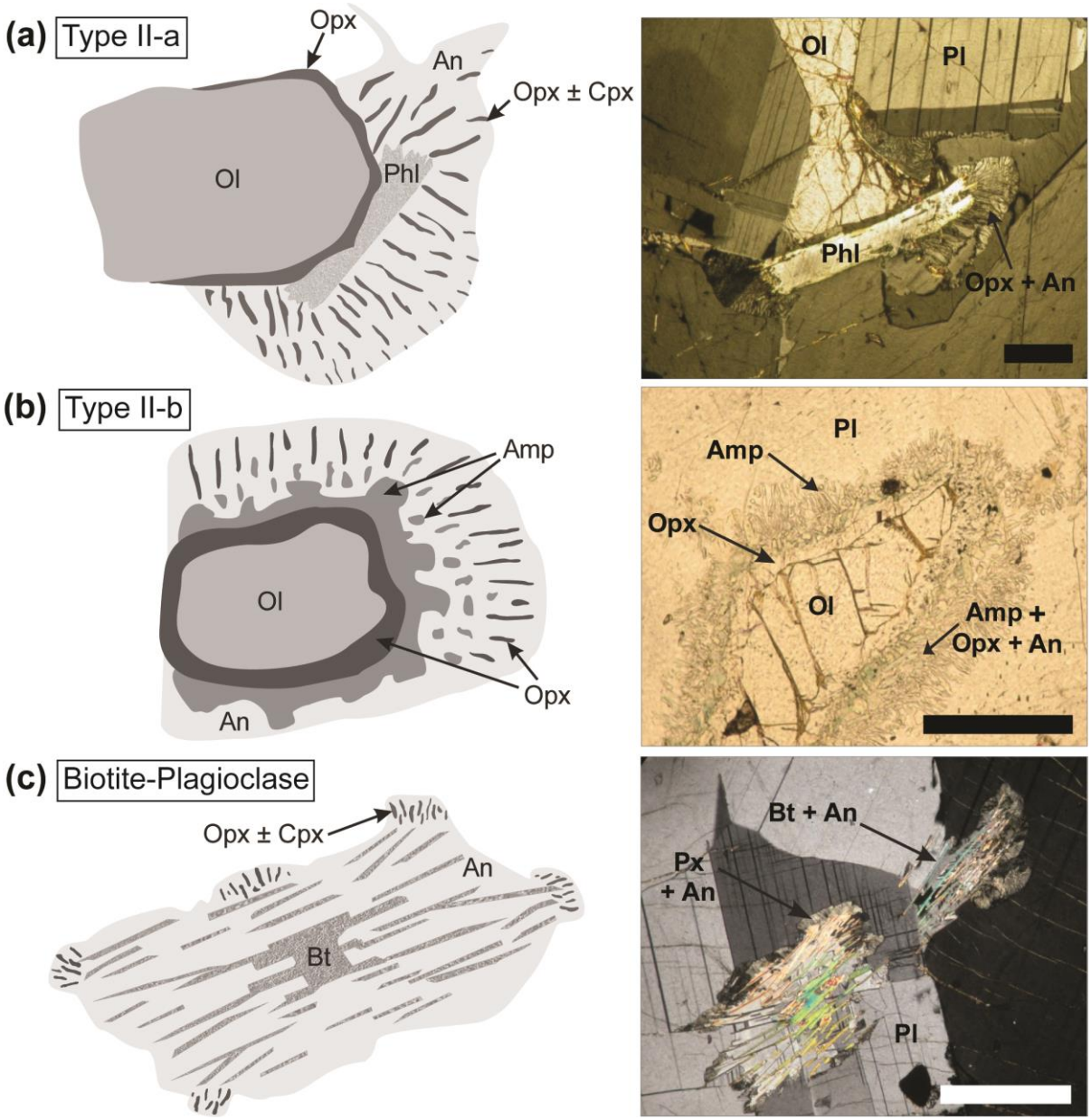

Fig. 4. a) Schematic diagram of a Type II-a symplectite (left), and crossed polarized photo micrograph (right) of a Type II-a symplectite, rooted to phlogopite adjacent to an olivine primocryst from sample 9-2258, MCU I. b) Schematic diagram of a Type II-b symplectite (left), and plane polarized photo micrograph (right) of a typical Type II-b symplectite from

sample ON-07-77, MCU III. c) Schematic diagram of a typical biotite-plagioclase symplectite (left), and crossed polarized photo micrograph (right) of a typical biotite-plagioclase symplectite from sample 8-689, MCU II. Opx = orthopyroxene, Cpx = clinopyroxene, An = anorthitic plagioclase, Pl = primocryst plagioclase, Phl = phlogopite, Ol = olivine, Amp = amphibole, Bt = biotite , Px = pyroxene (composition unknown). All scale bars are 1 mm long.

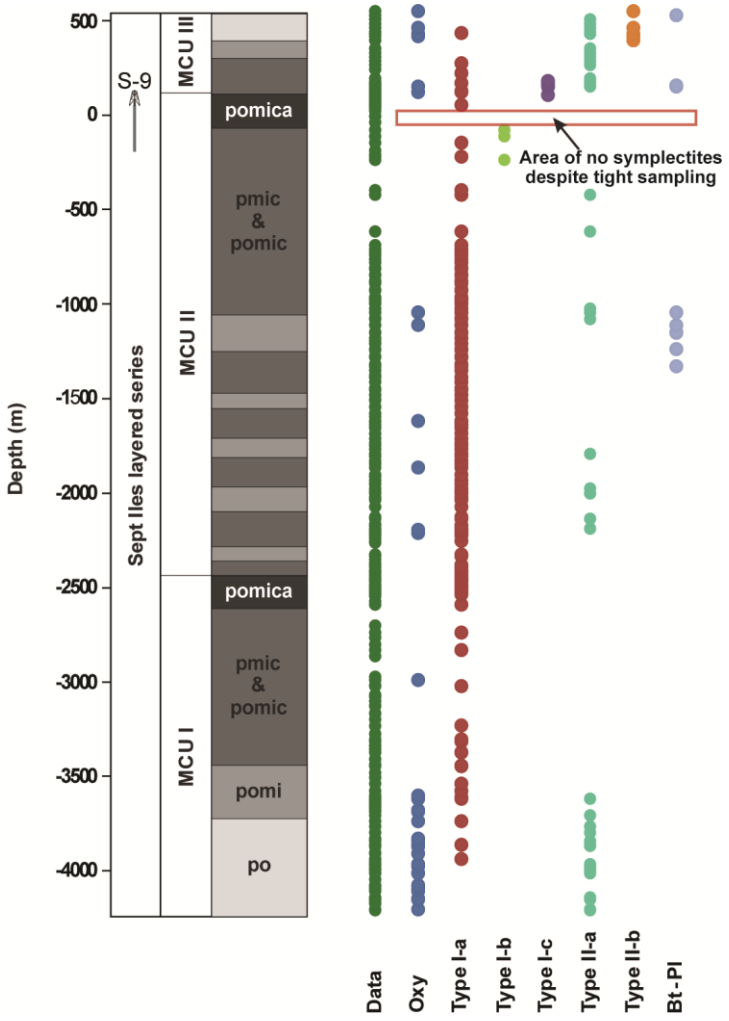

Fig. 5. Schematic stratigraphic section of the Sept Iles Layered Series, showing the megacyclic units (MCU) on the left with the cumulus assemblages in various shades of grey (modified from Namur *et al.*, 2012*a*). The 0 metre level corresponds to the lowest sample

with cumulus apatite in MCU II. The stratigraphic positions of all data points collected in this study are present in green, with the different types of symplectites labelled in various colours. See text for abbreviations of cumulus assemblages. Bt = biotite, Pl = plagioclase.

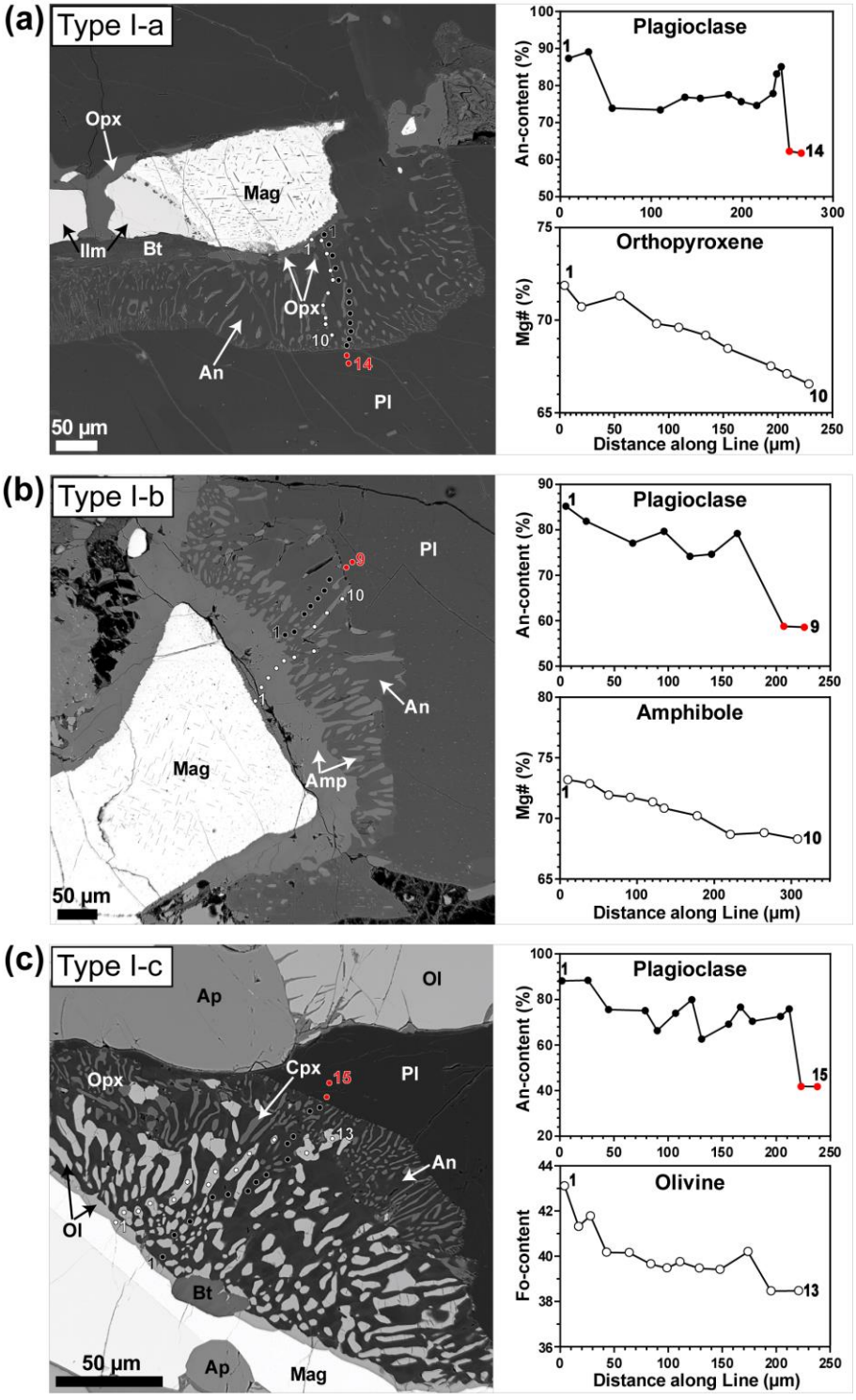

Fig. 6.

BSE images of Type I symplectites. For all images, dots indicate microprobe data points (see graphs). Red dots = primocryst values, black dots = symplectite plagioclase values, white dots = symplectite orthopyroxene (a), amphibole (b), or olivine (c) values.

a) *Left:* BSE image of a Type I-a symplectite from sample 8-689, MCU II. Note the wisps of fluctuating anorthite content (based on changes in grey scale) in the upper right of the image. *Right:* Graph of An-content of plagioclase (above) and Mg# of orthopyroxene (below) vs. distance along growth direction in the same sample. Note the difference of 29 mol.% between the most anorthitic symplectic plagioclase and the primocryst values, whereas the Mg# of the orthopyroxene only decreases by ~6 mol.% throughout growth of the symplectite.

b) *Left:* BSE image of a Type I-b symplectite from sample ON-07-152, MCU II. *Right:* Graph of An-content of plagioclase (above) and Mg# of amphibole (below) vs. distance along growth direction in the same sample. Note the 27 mol.% difference between primocryst plagioclase and the highest symplectite anorthite content, but only a 5 mol.% difference in Mg# between the most primitive and the most evolved amphibole vermicule in the symplectite.

c) *Left:* BSE image of a Type I-c symplectite from sample S9-57.5, top of MCU II. *Right:* Graph of An-content of plagioclase (above) and Fo-content of olivine (below) vs. distance along symplectite growth direction for the same sample. Note the significant 48 mol.% difference in An-content between primocryst and most primitive symplectite plagioclase, vs. the decrease of only ~4 mol.% in Fo-content of olivine in the symplectite along the growth direction.

Ilm = ilmenite, Mag = magnetite, Bt = biotite, Opx = orthopyroxene, An = anorthitic plagioclase, Pl = primocryst plagioclase, Amp = amphibole (magnesio-hornblende), Ol = olivine, Ap = apatite, Cpx = clinopyroxene.

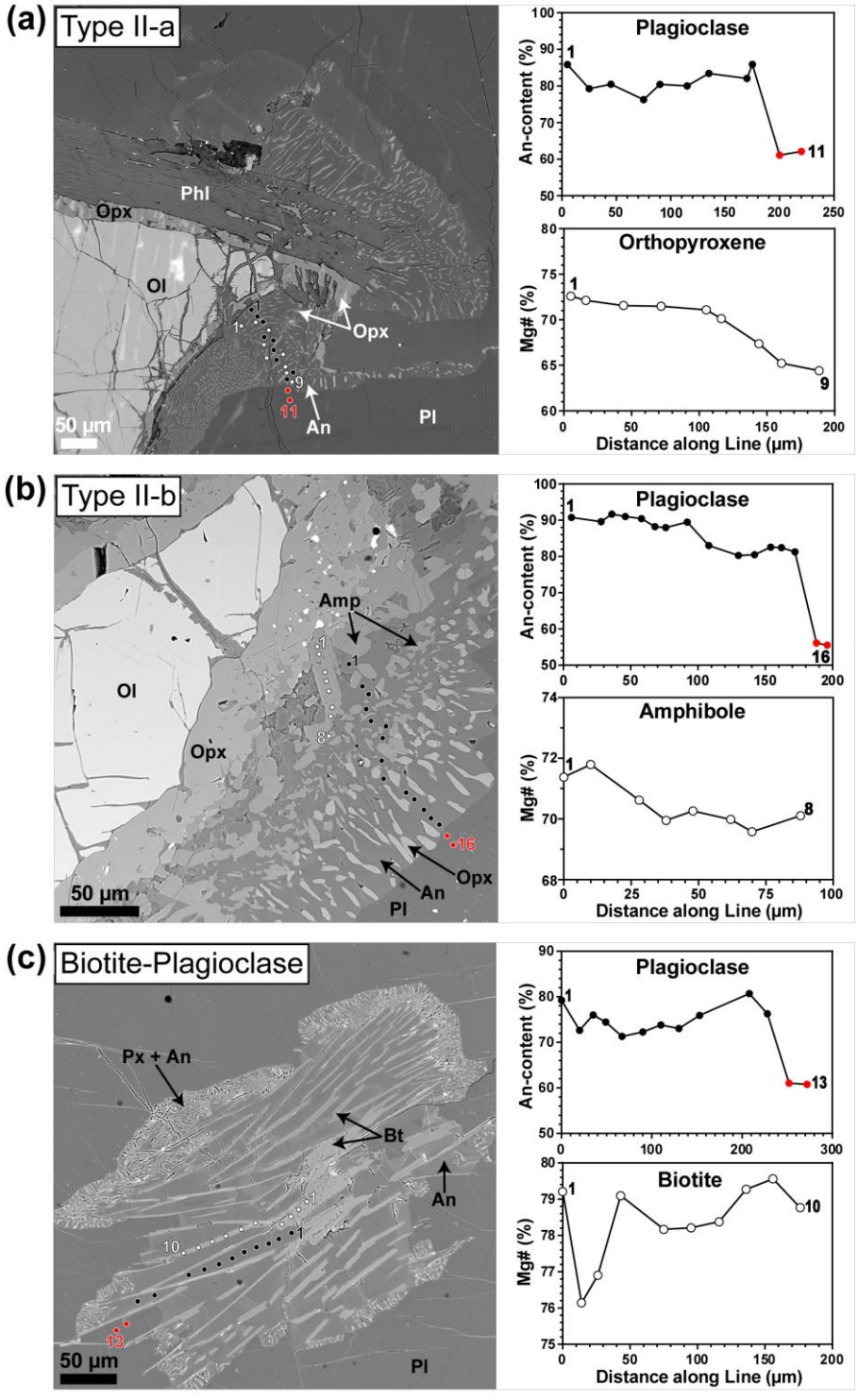

Fig. 7.

BSE images of Type II and biotite-plagioclase symplectites. For all images, dots indicate microprobe data points (see graphs). Red dots = primocryst values, black dots = symplectite plagioclase values, white dots = symplectite orthopyroxene (a), amphibole (b), or biotite (c) values.

a) *Left:* BSE image of a Type II-a symplectite from sample 9-2258, MCU I. The symplectite is composed of orthopyroxene + anorthite, and is rooted to either phlogopite (top right) or orthopyroxene rims around olivine primocrysts (bottom left). *Right:* Graph of An-content of plagioclase (above) and Mg# of orthopyroxene (below) vs. distance along growth direction for the same sample. Note the difference of ~24 mol.% in plagioclase composition between the symplectite and the primocryst, with only an 8 mol.% decrease in Mg# of the orthopyroxene along the growth direction of the symplectite.

b) *Left:* BSE image of a Type II-b symplectite from sample ON-07-77, MCU III. *Right:* Graph of An-content of plagioclase (above) and Mg# of amphibole (below) vs. distance along growth direction for the same sample. Note the difference of 35 mol.% between the symplectic plagioclase and the primocryst plagioclase, whereas the Mg# of amphibole decreases only ~2.5 mol.% along the growth direction of the amphibole vermicules.

c) *Left:* BSE image of biotite-plagioclase symplectites grading outwards into pyroxene-plagioclase symplectites from sample 8-689, MCU II. *Right:* Graph of plagioclase anorthite content (above) and Mg# of biotite (below) vs. distance (from inside to outside) in a biotite-plagioclase symplectite from the same sample. Note the difference of ~20 mol.% between the symplectic plagioclase and the primocryst plagioclase, whereas the Mg# of the biotite only varies by ~3 mol.%.

An = anorthitic plagioclase, Pl = primocryst plagioclase, Opx = orthopyroxene, Phl = phlogopite, Ol = olivine, Amp = amphibole, Bt = biotite, Px = pyroxene (composition unknown).

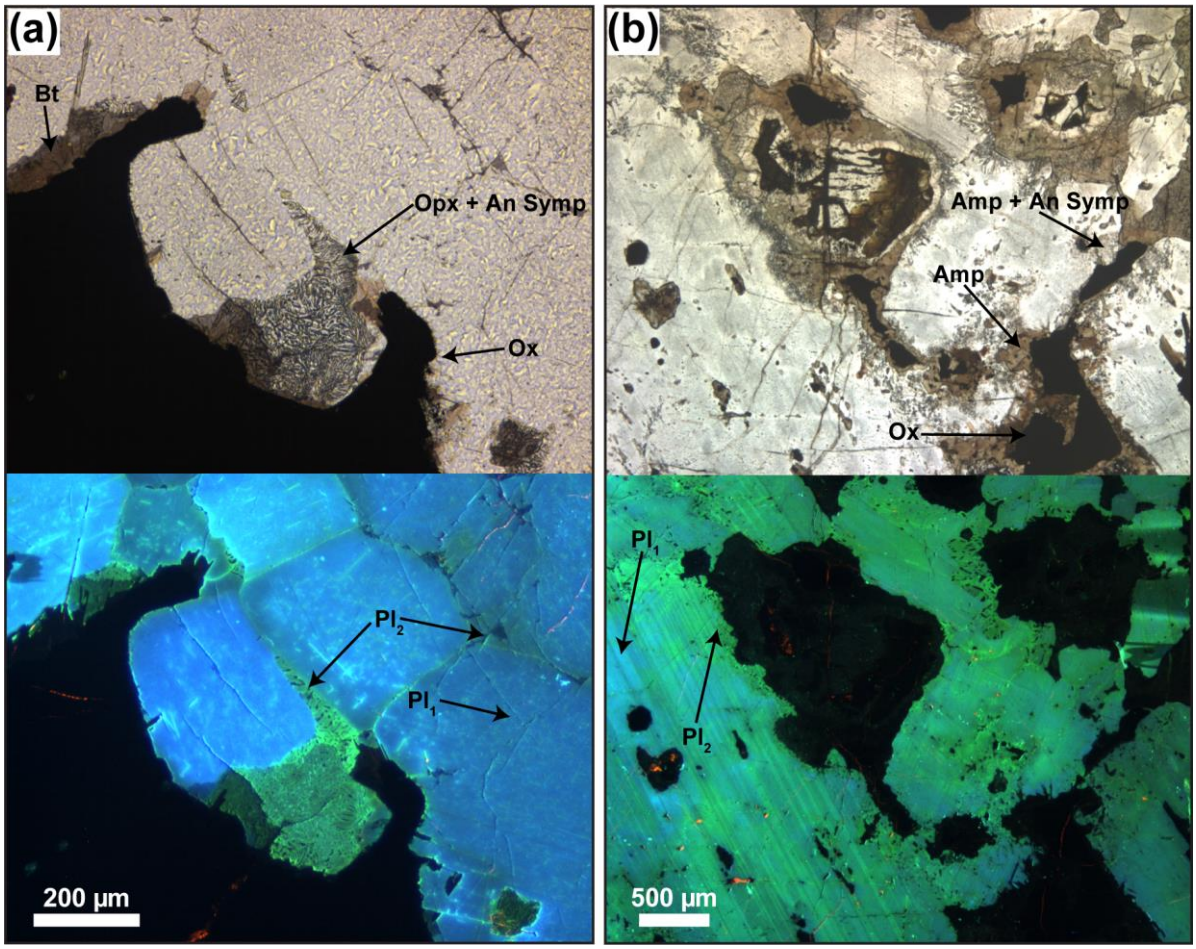

Fig. 8. a) Plane polarized photo micrograph (above) of a reactive Type I-a symplectite in sample 8-1838.5, MCU II. Below: Same area viewed under CL, showing green luminescing (anorthitic) plagioclase along grain boundaries as well as in the symplectite. b) Plane polarized photo micrograph (above) of sample ON-07-102 from MCU III, showing irregularly structured amphibole-rich symplectites. Below: Same image under CL, showing pervasive bright green luminescence throughout plagioclase primocrysts as well as along grain boundaries. Bt = biotite, Opx = orthopyroxene, An = anorthitic plagioclase, Symp =

symplectite, Ox = Fe-Ti oxide (magnetite ± ilmenite), Pl_1 = primocryst plagioclase, Pl_2 = replacement (anorthitic) plagioclase, Amp = amphibole.

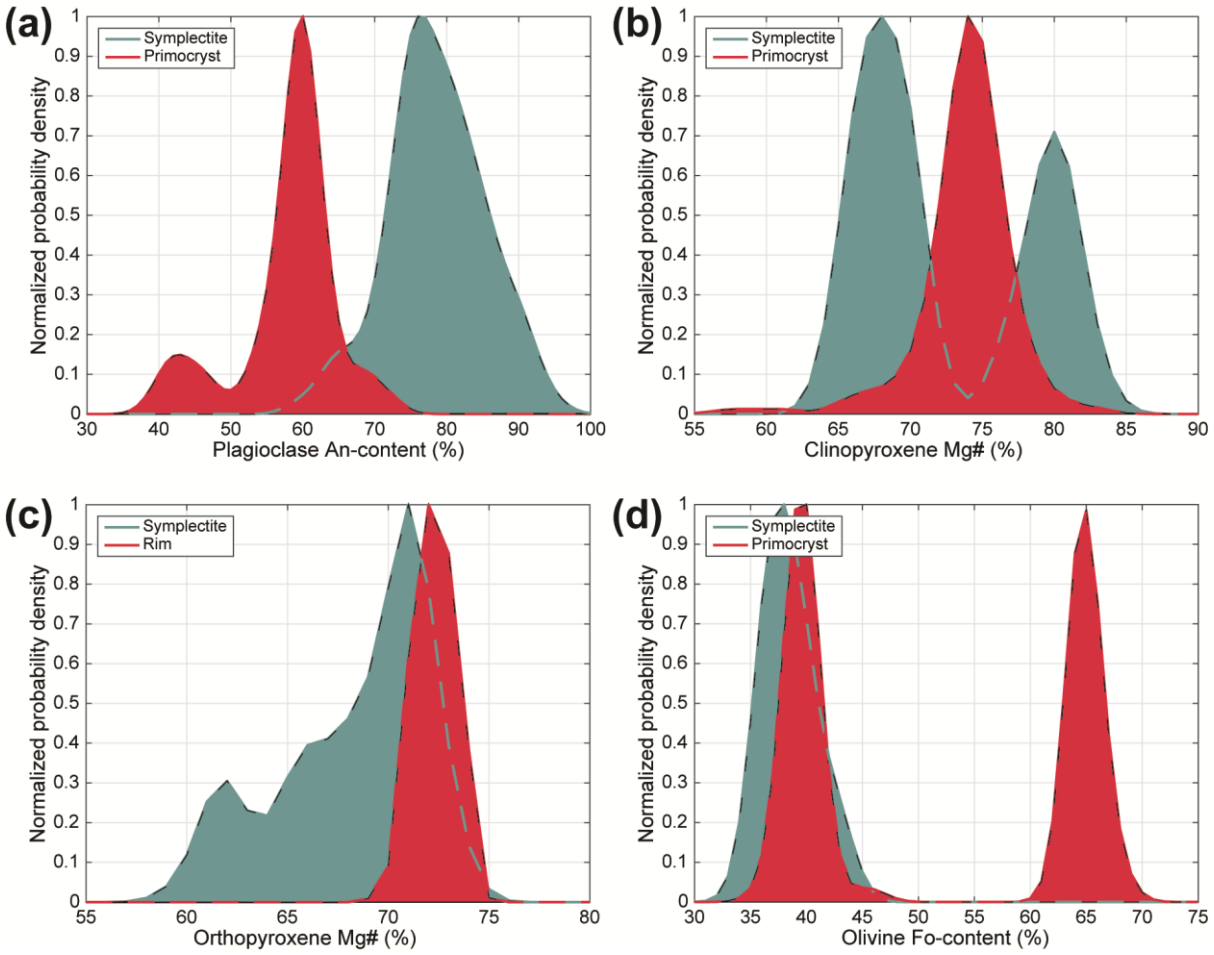

Fig. 9. a) Histogram (normalized probability density) showing the variation in primocryst (red) and symplectite (green) plagioclase anorthite contents from the Sept Iles Layered Series, showing significantly more anorthitic plagioclase in the symplectites. b) Histogram showing the variation in clinopyroxene primocryst composition (red) and symplectite composition (green). c) Histogram showing the variation in compositions between orthopyroxene rims (red) and symplectites (green). Note that there were no orthopyroxene primocrysts to measure in the Sept Iles Layered Series. d) Histogram showing the variation in Fo-content from primocryst olivine (red) and symplectite olivine (green) from the Sept Iles Layered Series.

Note that the olivine data between 35-45% was taken from very evolved rocks at the top of MCU-II and is therefore not representative of the Sept Iles Layered Series as a whole.

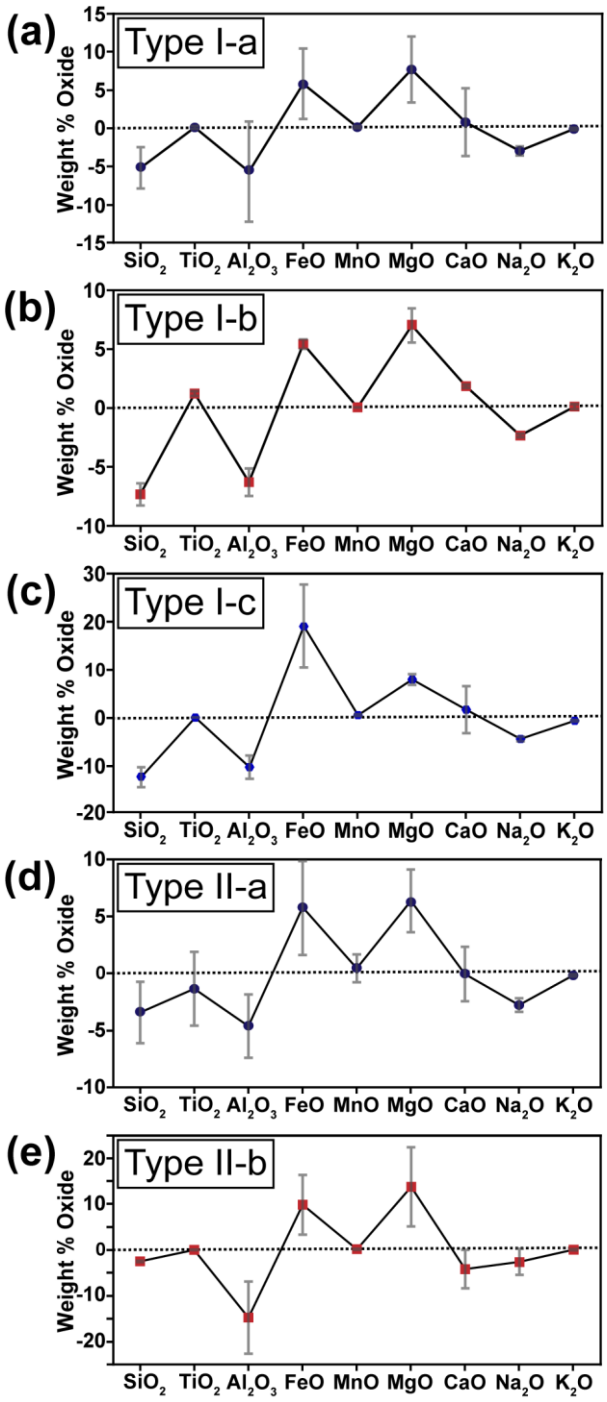

Fig. 10. Average mass balance analyses for a) Type I-a; b) Type I-b; c) Type I-c; d) Type II-a; and e) Type II-b symplectites, showing net losses and gains of major elements. Error bars are

1 standard deviation. For the mass balance analyses, bulk compositions of analysed symplectites were calculated based on averaged microprobe data. These compositions were then compared to the composition of the replaced plagioclase primocrysts to determine which elements were added or removed during reaction.

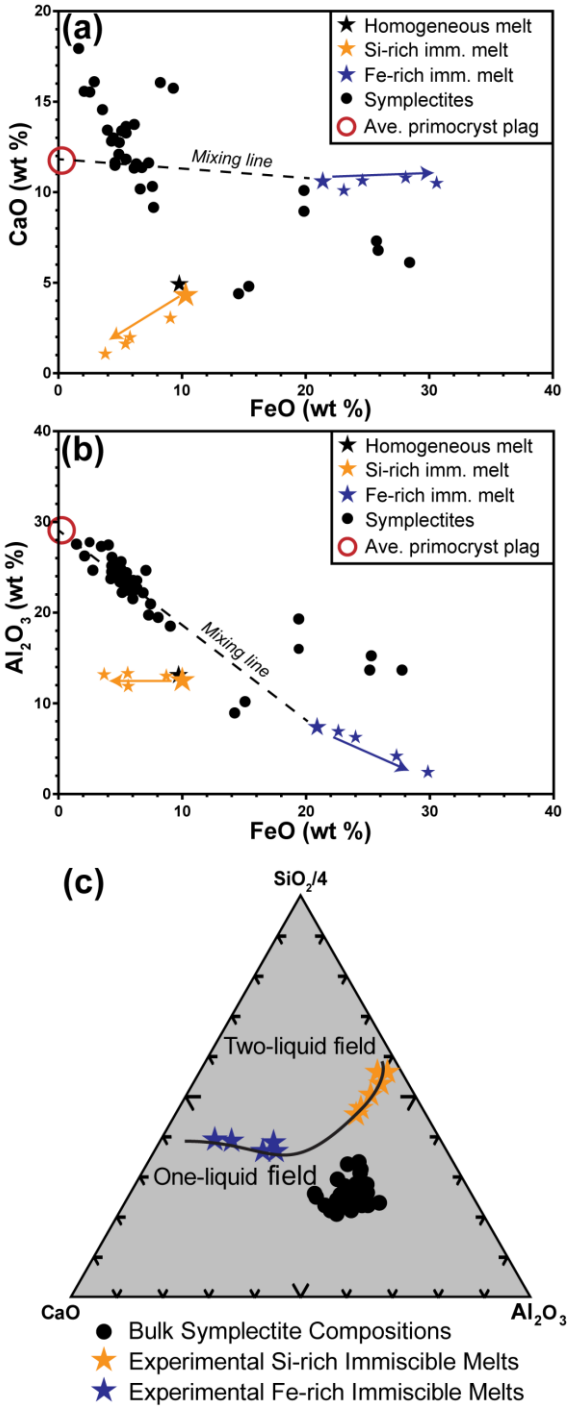

Fig. 11. Plot of a) CaO vs. FeO and b) Al_2O_3 vs. FeO for bulk symplectite compositions (black circles), Si-rich immiscible melt compositions (orange stars), Fe-rich immiscible melt compositions (blue stars), and the homogeneous melt composition just before immiscibility (black star), from the Sept Iles Layered Series. Larger stars represent the immiscible melts produced at the highest temperature (onset of immiscibility) while the smaller stars represent subsequent melts produced at lower temperatures. The direction of evolution of the Si-rich and Fe-rich melts after liquid immiscibility are labelled with coloured arrows. Red circles represent average primocryst plagioclase compositions. Black dashed lines represent the mixing line if plagioclase primocrysts were mixed with various proportions of the Fe-rich liquid. Values for all melts are from Charlier & Grove (2012). c) Compositions of Si-rich and Fe-rich immiscible melts projected onto a ternary diagram, creating the division between the one-liquid and two-liquid fields, with bulk symplectite compositions from the Sept Iles Layered Series labelled as black circles.

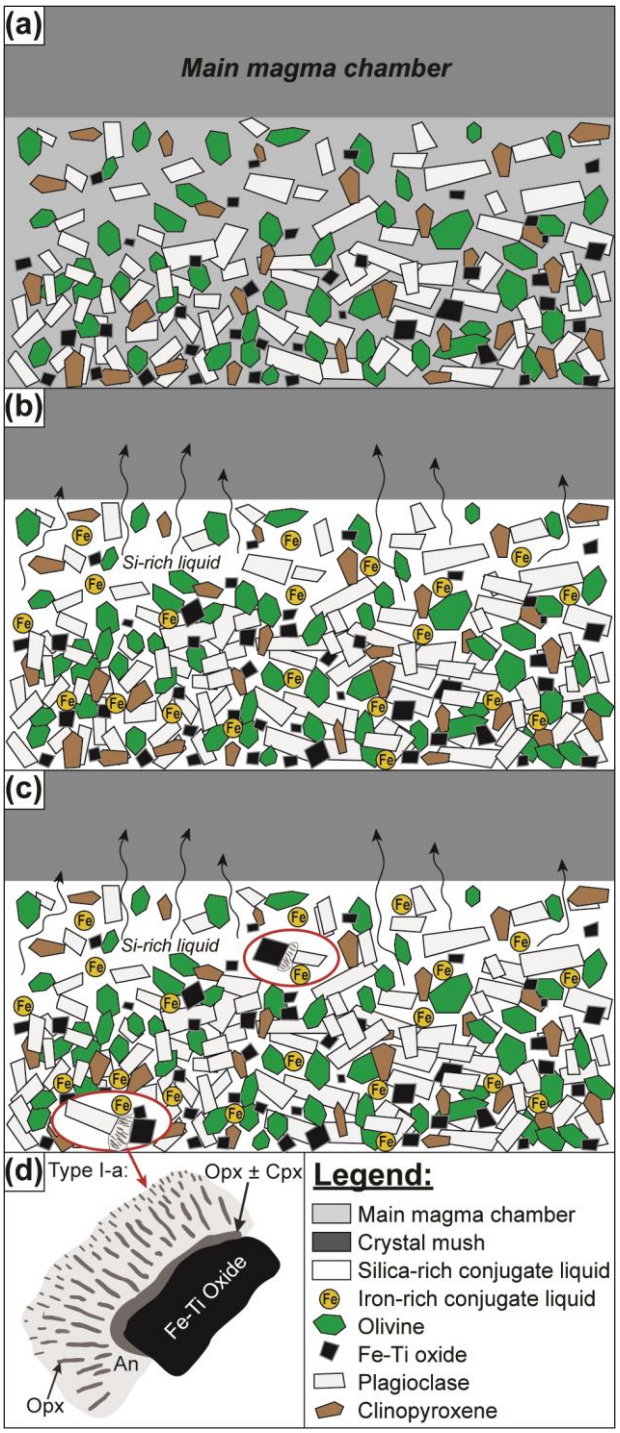

Fig. 12. Schematic diagram of a crystal mush undergoing separation into Si-rich and Fe-rich conjugates, resulting in the formation of symplectites. a) Primocryst grains accumulate and form a crystal mush at the bottom of the magma chamber. b) Si-rich liquid and Fe-rich liquid (yellow droplets) separate as a consequence of silicate liquid immiscibility. Driven by its low density, the more abundant Si-rich conjugate ascends and leaves the crystal mush. c)

Formation of Type I-a (anhydrous) symplectites as a consequence of reaction between plagioclase primocrysts and the remaining Fe-rich immiscible conjugate. d) Schematic diagram of a Type I-a symplectite that forms as a result of the processes indicated in (a) through (c).

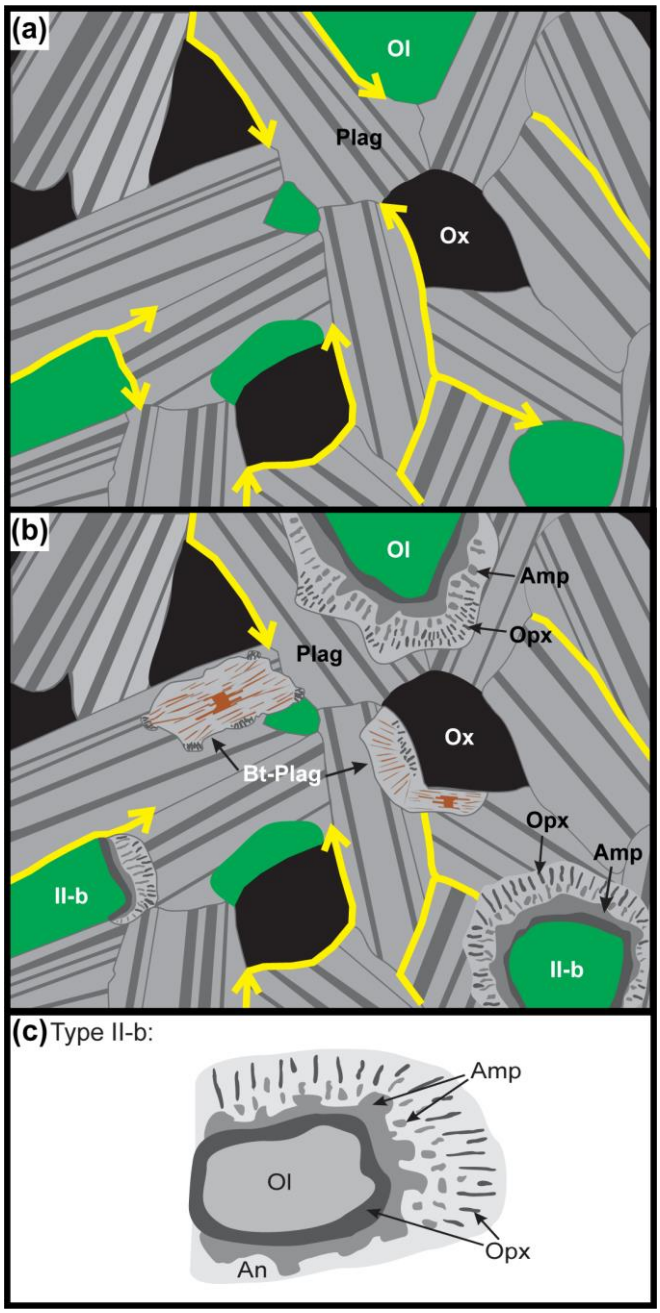

Fig. 13. Schematic diagram of the general proposed process for reactive symplectite formation, showing formation of hydrous Type II-b and biotite-plagioclase symplectites. a)

Fluid (in yellow), either melt or hydrous fluid, reacting adjacent to mafic primocrysts along grain boundaries. b) After reaction and dissolution of plagioclase, symplectites are formed from disequilibrium reactions in an open system. c) Schematic diagram of a Type II-b symplectite that formed as a result of the process indicated above. Note: symplectites are not drawn to scale, but are drawn so the vermicules can be seen clearly. Also, symplectite types do not all occur in the same rock samples. Ol = olivine, Pl = plagioclase, Opx = orthopyroxene, Ox = Fe-Ti oxide (magnetite ± ilmenite), Bt = biotite, Amp = amphibole, An = anorthitic plagioclase.

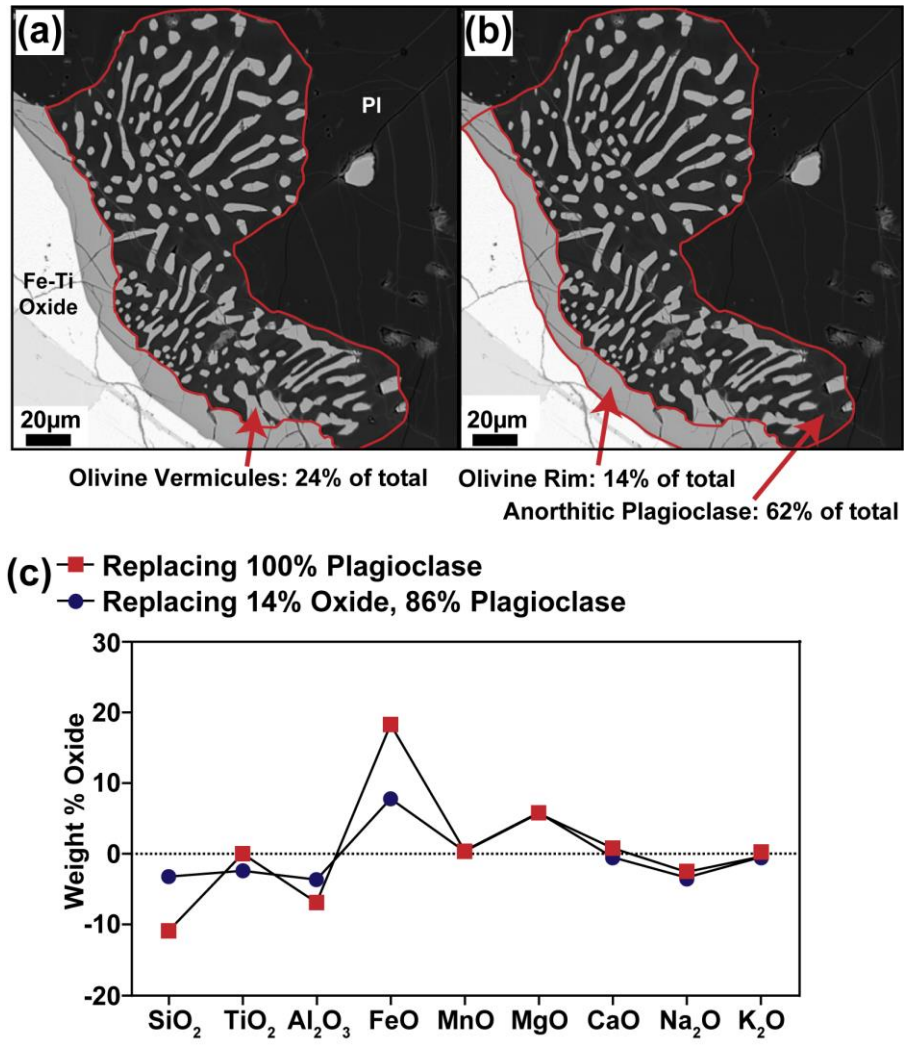

Supplementary Figure 1. An example of a Type I-c symplectite (sample S9-33.3, MCU II), measured with the original grain boundary a) at the edge of the olivine rim (where the

symplectite replaces 100% plagioclase) and b) with the original grain boundary at the current oxide boundary (meaning it replaces 14% Fe-Ti oxide as well). c) Mass balance calculations for the sample in a) and b), showing the minimal differences between calculations when the original grain boundary is measured at the current oxide boundary vs. being measured at the edge of the olivine rim. Pl = plagioclase, Fe-Ti Oxide = magnetite ± ilmenite.